Title
Higgs Physics and Cosmology

Author
Roberts, Alex

Publication Date
2016

Peer reviewed|Thesis/dissertation

Higgs Physics and Cosmology

By

Alex Roberts

A dissertation submitted in partial satisfaction of the
requirements of the degree of
Doctor of Philosophy
in
Physics
in the
Graduate Division
of the
University of California, Berkeley

Committee in charge:

Professor Yasunori Nomura, Chair
Professor Lawrence Hall
Professor Chung-Pei Ma

Spring 2016

Abstract

Higgs Physics and Cosmology

by

Alex Roberts

Doctor of Philosophy in Physics

University of California, Berkeley

Professor Yasunori Nomura, Chair

Recently, a new framework for describing the multiverse has been proposed which is based on the principles of quantum mechanics. The framework allows for well-defined predictions, both regarding global properties of the universe and outcomes of particular experiments, according to a single probability formula. This provides complete unification of the eternally inflating multiverse and many worlds in quantum mechanics. We elucidate how cosmological parameters can be calculated in this framework, and study the probability distribution for the value of the cosmological constant. We consider both positive and negative values, and find that the observed value is consistent with the calculated distribution at an order of magnitude level. In particular, in contrast to the case of earlier measure proposals, our framework prefers a positive cosmological constant over a negative one. These results depend only moderately on how we model galaxy formation and life evolution therein.

We explore supersymmetric theories in which the Higgs mass is boosted by the non-decoupling D-terms of an extended $U(1)_X$ gauge symmetry, defined here to be a general linear combination of hypercharge, baryon number, and lepton number. Crucially, the gauge coupling, g_X, is bounded from below to accommodate the Higgs mass, while the quarks and leptons are required by gauge invariance to carry non-zero charge under $U(1)_X$. This induces an irreducible rate, σBR, for $pp \to X \to \ell\ell$ relevant to existing and future resonance searches, and gives rise to higher dimension operators that are stringently constrained by precision electroweak measurements. Combined, these bounds define a maximally allowed region in the space of observables, (σBR, m_X), outside of which is excluded by naturalness and experimental limits. If natural supersymmetry utilizes non-decoupling D-terms, then the associated X boson can only be observed within this window, providing a model independent 'litmus test' for this broad class of scenarios at the LHC. Comparing limits, we find that current LHC results only exclude regions in parameter space which were already disfavored by precision electroweak data..

Recent LHC data, together with the electroweak naturalness argument, suggest that the top squarks may be significantly lighter than the other sfermions. We present supersymmetric models in which such a split spectrum is obtained through "geometries": being "close to" electroweak symmetry breaking implies being "away from" supersymmetry breaking, and vice versa. In particular, we present models in 5D warped spacetime, in which supersymmetry breaking and Higgs fields are located on the ultraviolet and infrared branes, respectively, and the top multiplets are localized to the infrared brane. The hierarchy of the Yukawa matrices can be obtained while

keeping near flavor degeneracy between the first two generation sfermions, avoiding stringent constraints from flavor and CP violation. Through the AdS/CFT correspondence, the models can be interpreted as purely 4D theories in which the top and Higgs multiplets are composites of some strongly interacting sector exhibiting nontrivial dynamics at a low energy. Because of the compositeness of the Higgs and top multiplets, Landau pole constraints for the Higgs and top couplings apply only up to the dynamical scale, allowing for a relatively heavy Higgs boson, including $m_h = 125$ GeV as suggested by the recent LHC data. We analyze electroweak symmetry breaking for a well-motivated subset of these models, and find that fine-tuning in electroweak symmetry breaking is indeed ameliorated. We also discuss a flat space realization of the scenario in which supersymmetry is broken by boundary conditions, with the top multiplets localized to a brane while other matter multiplets delocalized in the bulk.

Dedicated to my parents, Almut and Lutz.

Grateful also to you, Craig.

Love matters.

Acknowledgments

I would like to thank my advisor, Yasunori Nomura. I'm grateful for the opportunity to be able to work with him. Our time working together at Berkeley and Santa Barbara has been fun. He was good at teaching the material and involved Grant and I in discussing the direction of our research approach. He agreed to pursue a promising idea when other professors would not have been interested and it ended up being an important part of our publication (publication 1 in the previous section).

I also thank Grant Larsen for being a great office-mate in Santa Barbara and for many useful discussions. His odd sense of humour made him a great person to work with every day. I want to thank Sean Weinberg for being a good roommate at UC Berkeley. We didn't have a chance to work together but I was interested in what you were pursuing at the time. I enjoyed frequent discussions with Clifford Cheung both at UC Berkeley and the KITP in Santa Barbara. While I didn't stay for the entire 4 hour talk by your PhD adviser at the KITP, I learned a lot from discussing ideas on gravity and supersymmetry with you. I was very impressed by how much you can do in Mathematica and I am thankful for all the insights and discussions that eventually turned into a paper (publication 3 in the previous section). I want to thank Asimina Arvanitaki, Savas Dimopoulos, Joshua Ruderman and Satoshi Shirai for discussions and all the people in the particle group at UC Berkeley. The lunch meetings were great and we had a good time reading out paper abstracts and discussing ideas while we were having lunch. I also enjoyed the dinners with speakers that we had often. I had the opportunity to try raw squid and other delicacies and I only had to pay for the drinks.

I want to thank Prof. Christian Bauer for working with me on the GENEVA project, on the adaptive sampling of the Monte Carlo generator. I'm grateful for the opportunity to work with Simone Alioli and Jonathan Walsh on this project and to even be able to teach a new post-doc on the details of what I had been doing. I want to thank Prof. Holger Müller for working with me for a summer on his research.

Contents

List of Tables

List of Figures

1 Introduction

1.1 The Cosmological Constant in the Quantum Multiverse

An explanation of a small but nonzero cosmological constant is one of the major successes of the picture that our universe is one of the many different universes in which low energy physical laws take different forms [24]. Such a picture is also suggested theoretically by eternal inflation [25] and the string landscape [26]. This elegant picture, however, has been suffering from the predictivity crisis caused by an infinite number of events occurring in eternally inflating spacetime. To make physical predictions, we need to deal with these infinities and define physically sensible probabilities [27].

Recently, a well-defined framework to describe the eternally inflating multiverse has been proposed based on the principles of quantum mechanics [28]. In this framework, the multiverse is described as quantum branching processes viewed from a single "observer" (geodesic), and the probabilities are given by a simple Born-like rule applied to the quantum state describing the entire multiverse. Any physical questions—either regarding global properties of the universe or outcomes of particular experiments—can be answered by using this single probability formula, providing *complete unification* of the eternally inflating multiverse and many worlds in quantum mechanics. Moreover, the state describing the multiverse is defined on the "observer's" past light cones bounded by (stretched) apparent horizons; namely, consistent description of the *entire* multiverse is obtained in these limited spacetime regions. This leads to a dramatic change of views on spacetime and gravity.

In this paper we present a calculation of the probability distribution of the cosmological constant in this new framework of the quantum multiverse.[1] We fix other physical parameters and ask what values of the cosmological constant Λ we are likely to observe. In Section 2.1 we begin by reviewing the proposal of Ref. [28], and we then explain how cosmological parameters can be calculated in Section 2.2. While the framework itself is well-defined, any practical calculation is necessarily approximate, since we need to model "experimenters" who actually make observations. In our context, we need to consider galaxy formation and life evolution therein, which we will do in Section 2.3. We present the result of our calculation in Section 2.4. We find that, in contrast to the case with some earlier measures [34], the measure of Ref. [28] does not lead to unwanted preference for a negative cosmological constant—in fact, a positive value is preferred. We find that a simple anthropic condition based on metallicity of stars is sufficient to make the calculated distribution consistent with the observed value at an order of magnitude level. We conclude in Section 4.5.

Appendix A lists formulae for galaxy formation used in our analysis. Appendix B discusses

[1] For earlier studies of the cosmological constant in the context of geometric cutoff measures, see Refs. [29 – 33].

the anthropic condition coming from metallicity of stars.

1.2 Higgs Mass from D-Terms: a Litmus Test

Vital clues to the nature of electroweak symmetry breaking have emerged from the LHC. The bulk of the standard model (SM) Higgs mass region has been excluded at 95% CL [1, 2], leaving a narrow window 123 GeV $< m_h <$ 128 GeV in which there is a modest excess of events consistent with $m_h \simeq 125$ GeV. As is well-known, such a mass can be accommodated within the minimal supersymmetric standard model (MSSM) but this requires large A-terms or very heavy scalars, which tend to destabilize the electroweak hierarchy and undermine the original naturalness motivation of supersymmetry (SUSY) [3, 4, 5]. Post LEP, however, a variety of strategies were devised in order to lift the Higgs mass. In these models the Higgs quartic coupling is boosted: either at tree level, via non-decoupling F-terms [6, 7, 8] and D-terms [9, 10], or radiatively, via loops of additional matter [11, 12]. Already, a number of groups have redeployed these model building tactics in light of the recent LHC Higgs results [5, 13, 14, 15].

The present work explores non-decoupling D-terms in gauge extensions of the MSSM. Our aim is to identify the prospects for observing this scenario at the LHC in a maximally model independent way. To begin, consider the MSSM augmented by an arbitrary flavor universal $U(1)_X$, which may be parameterized as a linear combination of hypercharge Y, Peccei-Quinn number PQ, baryon number B, and lepton number L. The Higgs must carry X charge if the corresponding D-terms are to contribute to the Higgs potential, so X must have a component in Y or PQ. However, PQ forbids an explicit μ term, so gauging PQ requires a non-trivial modification to the Higgs sector which is highly model dependent. To sidestep this complication we ignore PQ and study the otherwise general space of $U(1)_X$ theories consistent with a μ term,

$$X \;=\; Y + pB - qL, \tag{1}$$

where the normalization of X relative to Y has been absorbed into the sign and magnitude of the gauge coupling, g_X. We impose no further theoretical constraints, but will comment later on anomalies, naturalness, and perturbative gauge coupling unification. As we will see, the ultraviolet dynamics, e.g. the precise mechanism of gauge symmetry and SUSY breaking, will be largely irrelevant to our analysis.

We constrain $U(1)_X$ with experimental data from resonance searches, precision electroweak measurements, and Higgs results. Remarkably, non-trivial limits can be derived without exact knowledge of seemingly essential parameters like g_X, p, and q. This is possible because g_X is bounded *from below* by the mass of the Higgs while the couplings of the X boson to quarks, leptons, and the Higgs are *non-zero for all* values of p and q. As a result, for a fixed value of the X boson mass, m_X, the theory predicts an irreducible rate, σBR, for the process $pp \to X \to \ell\ell$

(relevant to direct searches) and an irreducible coupling of X to the Higgs and leptons (relevant to precision electroweak data).

Combining limits, we derive a maximal allowed region in the space of observables, $(\sigma \mathrm{BR}, m_X)$, outside of which is either unnatural or in conflict with experimental bounds, as shown in Figs. 6 and 7. If non-decoupling D-terms indeed play a role in boosting the Higgs mass, then the X boson can only be observed within this allowed region—a 'litmus test' for this general class of theories. Furthermore, we find that for natural SUSY, i.e. $m_{\tilde{t}} \lesssim 500$ GeV, resonance searches from the LHC [16] are not yet competitive with existing precision electroweak constraints.

In Sec. 3.1 we define our basic setup. Applying the constraints of gauge symmetry and SUSY, we derive a general expression for the Higgs potential arising from non-decoupling D-terms. Afterwards, in Sec. 3.2 we compute the Higgs mass and the couplings of the MSSM fields to the X boson. We then impose experimental limits and suggest a simple litmus test for non-decoupling D-terms. We conclude in Sec. 3.3.

1.3 Supersymmetry with Light Stops

One of the strongest motivations for weak scale supersymmetry is the possibility of making electroweak symmetry breaking "natural," i.e. a generic parameter region of the theory reproduces observed electroweak phenomena. With the Higgs potential $V(h) = m^2 h^\dagger h + \lambda (h^\dagger h)^2/4$, the minimization of the potential leads to $v \equiv \langle h \rangle = \sqrt{-2m^2/\lambda}$ and

$$\frac{m_h^2}{2} = -m^2, \tag{2}$$

where m_h is the physical Higgs boson mass. In the Standard Model (SM) a generic size of $|m^2|$ is expected to be at a scale where the theory breaks down, while in supersymmetric models

$$m^2 = |\mu|^2 + \tilde{m}_h^2, \tag{3}$$

where μ and $\tilde{m}_h^2$ are the supersymmetric and supersymmetry-breaking masses for the Higgs field. Therefore, as long as these parameters are both of order the weak scale, the theory can naturally accommodate electroweak symmetry breaking.

Improved experimental constraints over the past decades, however, have cast doubt on this simple picture. In softly broken supersymmetric theories, supersymmetry-breaking masses are affected by each other through renormalization group evolution; in particular, $\tilde{m}_h$ receives a contribution

$$\delta \tilde{m}_h^2 \simeq -\frac{3 m_t^2}{4\pi^2 v^2}\, m_{\tilde{t}}^2 \ln \frac{M_{\mathrm{mess}}}{m_{\tilde{t}}}, \tag{4}$$

where m_t and $m_{\tilde{t}}$ are the top quark and squark masses, and M_{mess} the scale at which supersymmetry breaking masses are generated. (Here, we have ignored possible scalar trilinear

interactions and set the left- and right-handed squark masses equal, for simplicity.) Requiring no more fine-tuning than Δ, Eqs. (2) and (3) lead to

$$m_{\tilde{t}} \lesssim 420 \text{ GeV} \left(\frac{m_h}{125 \text{ GeV}}\right) \left(\frac{20\%}{\Delta^{-1}}\right)^{1/2} \left(\frac{3}{\ln \frac{M_{\rm mess}}{m_{\tilde{t}}}}\right)^{1/2}. \tag{5}$$

On the other hand, recent observations at the LHC indicate:

- Generic lower bounds on the first two generation squark masses are about 1 TeV [50].
- There are hints of the SM-like Higgs boson with $m_h \simeq 125$ GeV [51].

Therefore, if the hints for the Higgs boson mass are true, then it strongly suggests that the squark masses have a nontrivial flavor structure, i.e. top squarks (stops) are light.[2]

The above observation has significant implications on an underlying model of supersymmetry breaking. This is especially because many existing models, including minimal supergravity, gauge mediation, and anomaly mediation, invoke flavor universality to avoid stringent constraints from the absence of large flavor violating processes. On the other hand, it has been realized that naturalness itself allows sfermions other than the stops (and the left-handed sbottom) to be significantly heavier than the value suggested by Eq. (5) [53, 54, 55, 56, 57, 58]. In this paper, we study a simple, general framework in which such superparticle spectra with light stops are obtained naturally.

One strategy to yield such light stop spectra is to arrange the theory in such a way that being "away" from electroweak symmetry breaking necessarily means being "close" to supersymmetry breaking, and vice versa. This makes the lighter generations (particles feeling smaller effects from electroweak symmetry breaking) obtain larger supersymmetry breaking masses, e.g. of order a few TeV, while keeping stops light. Strong constraints from flavor violation still require the first two generation sfermions to be flavor universal, but this can be achieved if these generations are both strongly localized to the supersymmetry breaking "site," and if mediation of supersymmetry breaking there is flavor universal. The setup described here is depicted schematically in Fig. 1.

A simple way to realize the above setup is through geometry. Suppose there is an extra dimension compactified on an interval, of which the Higgs and supersymmetry breaking fields h and X are localized at the opposite ends. The SM gauge, quark, and lepton multiplets propagate in the bulk. Now, if two generations are localized towards the "X brane" and (at least the quark

[2]One way of avoiding this conclusion is to invoke a significant mixing of the Higgs field with another scalar field; see [52]. In general, mixing of the SM-like Higgs field with another field can weaken the naive constraint, Eq. (5), obtained in the decoupling regime (at the cost of moderate cancellation in a scalar mass-squared eigenvalue). Another possibility is to have a relatively compressed superparticle spectrum, in particular a small mass splitting between the squarks and the lightest neutralino, in which case the lower bound on the (light generation) squark masses becomes weaker.

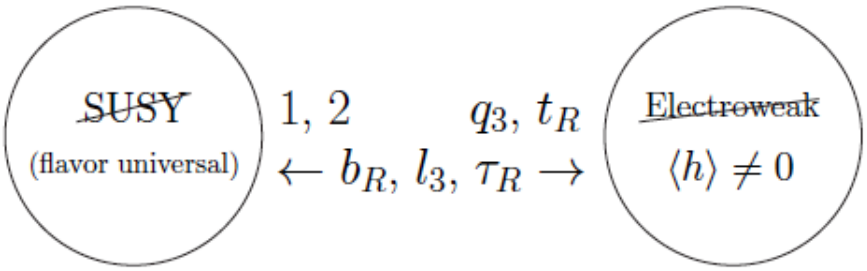

Figure 1: A basic scheme yielding light stop spectra. A theory has one "dimension," of which electroweak and supersymmetry breakings are "located" at the opposite ends. This dimension may be geometric or an effective one generated through dynamics. The first two generation fields are localized towards the supersymmetry breaking "site," obtaining flavor universal supersymmetry breaking masses and only small effects from electroweak symmetry breaking (small Yukawa couplings). On the other hand, top-quark multiplets are localized more towards the electroweak breaking "site," obtaining a large Yukawa coupling but only small supersymmetry breaking effects.

doublet and up-type quark of) the other generation is localized towards the "h brane," then it explains the (anti-)correlation between the spectrum of SM matter and its superpartners—the hierarchy of the Yukawa couplings are generated through the wavefunction overlap of SM matter with the h brane, while only the first two generation sfermions obtain significant supersymmetry breaking masses through interactions with the X brane.

Another manifestation of this is through dynamics—the "dimension" separating two breakings in Fig. 1 may be generated effectively as a result of strong (quasi-)conformal dynamics. Suppose there are elementary as well as composite sectors. In this case, particles in each sector interact with significant strength, but interactions involving both elementary and composite particles are suppressed by higher dimensions of composite fields. This can therefore be used to realize our setup, for example, by considering X and h to be elementary and composite fields, respectively. The SM matter fields are mixture of elementary and composite states—two generations being mostly elementary while the other mostly composite. In this way, the required pattern for the sfermion masses, as well as the hierarchical structure of the Yukawa couplings, are obtained. In fact, this picture can be related with the geometric picture described above. Since the strong, composite sector exhibits (approximate) conformality at high energies, the dynamics is well described by a warped extra dimension, using the AdS/CFT correspondence. (For applications of this idea in other contexts, see e.g. [59, 60, 61].)

In this paper, we present a class of models formulated in warped space, which can be interpreted either as a geometric or dynamical realization described above. In the next section,

we present the basic structure of the models and interpret them as composite Higgs-top models in the desert. We pay particular attention to how strong constraints from flavor violation are avoided while generating the Yukawa hierarchy. In Section 4.2, we analyze electroweak symmetry breaking and present sample superparticle spectra; we also give some useful formulae for the Higgs boson mass in the appendix. In section 4.4, we mention a realization of our scheme in a flat space extra dimension. We conclude in Section 4.5.

The configuration of supersymmetry breaking and matter/Higgs fields in our models is the same as that in "emergent supersymmetry" models considered before [62, 63, 64], where the masses of elementary superpartners $\tilde{m}$ are taken (much) above the scale of strong dynamics k'. In this picture, the quadratic divergence of the Higgs mass-squared parameter is regulated by a combination of composite Higgsinos/stops as well as higher resonances of the strong sector (Kaluza-Klein towers). Instead, our picture here is that the theory below the compositeness scale is the full supersymmetric standard model, $\tilde{m} < k'$, so that the quadratic divergence of the Higgs mass-squared is regulated by superpartner loops as in usual supersymmetric models—the strong sector simply plays a role of generating a light stop spectrum at some energy k'. This alleviates the problem of a potentially large D-term operator [63], intrinsic to the framework of Ref. [62, 63, 64].

Three interesting papers have recently considered light stops in supersymmetry [65, 66, 67], which are related to our study here. Ref. [65] discusses supersymmetric models in which the Higgs, top, and electroweak gauge fields are (partial) composites of a strong sector that sits at the bottom edge of the conformal window. This can be viewed as an explicit 4D realization of our warped 5D setup. (This "analogy" has also been drawn in that paper.) Ref. [66] considers the scheme of flavor mediation, where supersymmetry breaking is mediated through a gauged subgroup of SM flavor symmetries, leading to degenerate light-generation sfermions with light stops. Ref. [67] discusses light stops in the context of heterotic string theory.

2 The Cosmological Constant in the Quantum Multiverse

2.1 Probabilities in the Quantum Mechanical Multiverse

Here we review aspects of the framework of Ref. [28] which are relevant to our calculation. In this framework, the entire multiverse is described as a single quantum state as viewed from a single "observer" (geodesic). It allows us to make well-defined predictions in the multiverse (both cosmological and terrestrial), based on the principles of quantum mechanics.

Let us begin by considering a scattering process in usual (non-gravitational) quantum field theory. Suppose we collide an electron and a positron, with well-defined momenta and spins:

$|e^+e^-\rangle$ at $t = -\infty$. According to the laws of quantum mechanics, the evolution of the state is deterministic. In a relativistic regime, however, this evolution does *not* preserve the particle number or species, so we find

$$\Psi(t = -\infty) = \left|e^+e^-\right\rangle \quad \rightarrow \quad \Psi(t = +\infty) = c_e \left|e^+e^-\right\rangle + c_\mu \left|\mu^+\mu^-\right\rangle + \cdots , \tag{6}$$

when we expand the state in terms of the free theory states (which is appropriate for $t \to \pm\infty$ when interactions are weak). The Hilbert space of the theory is (isomorphic to) the Fock space

$$\mathcal{H} = \bigoplus_{n=0}^{\infty} \mathcal{H}_{1\mathrm{P}}^{\otimes n}, \tag{7}$$

where $\mathcal{H}_{1\mathrm{P}}$ is the single-particle Hilbert space. Various "final states," $|e^+e^-\rangle, |\mu^+\mu^-\rangle, \cdots$, in Eq. (6) arise simply because the time evolution operator causes "hopping" between different components of the Fock space in Eq. (7).

The situation in the multiverse is quite analogous. Suppose the universe was in an eternally inflating (quasi-de Sitter) phase Σ at some early time $t = t_0$. In general, the evolution of this state is *not* along the axes determined by operators local in spacetime. Therefore, at late times, the state is a superposition of different "states"

$$\Psi(t = t_0) = |\Sigma\rangle \quad \rightarrow \quad \Psi(t) = \sum_i c_i(t) \left|(\text{cosmic}) \text{ configuration } i\right\rangle , \tag{8}$$

when expanded in terms of the states corresponding to definite semi-classical configurations. The Hilbert space of the theory is (isomorphic to)

$$\mathcal{H} = \bigoplus_{\mathcal{M}} \mathcal{H}_{\mathcal{M}}, \qquad \mathcal{H}_{\mathcal{M}} = \mathcal{H}_{\mathcal{M},\mathrm{bulk}} \otimes \mathcal{H}_{\mathcal{M},\mathrm{horizon}}, \tag{9}$$

where $\mathcal{H}_{\mathcal{M}}$ is the Hilbert space for a fixed semi-classical spacetime $\mathcal{M}$, and consists of the bulk and horizon parts $\mathcal{H}_{\mathcal{M},\mathrm{bulk}}$ and $\mathcal{H}_{\mathcal{M},\mathrm{horizon}}$. (The quantum states are defined on the "observer's" past light cones bounded by apparent horizons.) The final state of Eq. (8) becomes a superposition of different semi-classical configurations because the evolution operator for $\Psi(t)$ allows "hopping" between different $\mathcal{H}_{\mathcal{M}}$ in Eq. (9).

As discussed in detail in Ref. [28], any physical question can be phrased as: "Given what we know about our past light cone, A, what is the probability of that light cone to have properties B as well?" This probability is given by

$$P(B|A) = \frac{\int dt \, \langle\Psi(t)| \, \mathcal{O}_{A\cap B} \, |\Psi(t)\rangle}{\int dt \, \langle\Psi(t)| \, \mathcal{O}_A \, |\Psi(t)\rangle}, \tag{10}$$

assuming that the multiverse is in a pure state $|\Psi(t)\rangle$. (The mixed state case can be treated similarly.) Here, $\mathcal{O}_A$ is the projection operator

$$\mathcal{O}_A = \sum_i |\alpha_{A,i}\rangle \langle\alpha_{A,i}| , \tag{11}$$

where $|\alpha_{A,i}\rangle$ represents a set of orthonormal states in the Hilbert space of Eq. (9), i.e. possible past light cones, that satisfy condition A (and similarly for $\mathcal{O}_{A\cap B}$). Despite the fact that the t integrals in Eq. (10) run from $t = t_0$ to ∞, the resulting $P(B|A)$ is well-defined, since $|\Psi(t)\rangle$ is continually "diluted" into supersymmetric Minkowski states [28].

The formula in Eq. (10) (or its mixed state version) can be used to answer questions both regarding global properties of the universe and outcomes of particular experiments. This, therefore, provides complete unification of the two concepts: the eternally inflating multiverse and many worlds in quantum mechanics [28].[3] To predict/postdict physical parameters x, we need to choose A to select the situation for "premeasurement" *without* conditioning on x. We can then use various different values (ranges) of x for B, to obtain the probability distribution $P(x)$. In the next section, we discuss this procedure in more detail, in the context of calculating the probability distribution of the vacuum energy, $x = \rho_\Lambda \equiv \Lambda/8\pi G_N$.

2.2 Predicting/Postdicting Cosmological Parameters

In order to use Eq. (10) to predict/postdict physical parameters, we need to know the relevant properties of both the state $|\Psi(t)\rangle$ (or its bulk part $\rho_{\rm bulk} \equiv {\rm Tr}_{\rm horizon}\, |\Psi(t)\rangle \langle\Psi(t)|$) and the operators $\mathcal{O}_A$ and $\mathcal{O}_{A\cap B}$. Here we discuss them in turn.

In general, the state $|\Psi(t)\rangle$ depends on the dynamics of the multiverse, including the scalar potential in the landscape, as well as the initial condition, e.g. at $t = t_0$. Given limited current theoretical technology, this introduces uncertainties in predicting physical parameters. However, there are certain cases in which these uncertainties are under control. Consider $x = \rho_\Lambda$. We are interested only in a range a few orders of magnitude around $\rho_{\Lambda,{\rm obs}} \simeq (0.0024\ {\rm eV})^4$ [36], which is tiny compared with the theoretically expected range $-M_{\rm Pl}^4 \lesssim \rho_\Lambda \lesssim M_{\rm Pl}^4$. Therefore, unless the multiverse dynamics or initial condition has a special correlation with the value of the vacuum energy in the standard model (SM) vacua, we expect that the probabilities of having these vacua in $|\Psi(t)\rangle$ is statistically uniform in x within the range of interest. (This corresponds to the standard assumption of statistical uniformity of the prior distribution of ρ_Λ [24].) The distribution of $x = \rho_\Lambda$ is then determined purely by the dynamics *inside* the SM universes, i.e., the probability of developing experimenters who actually make observations of the vacuum energies.

Let us now turn to the operators $\mathcal{O}_A$ and $\mathcal{O}_{A\cap B}$. In order to predict the value of the vacuum energy which a given experimenter will observe, we need to choose $\mathcal{O}_A$ to select a particular

[3]The claim that the multiverse and many worlds are the same has also been made recently in Ref. [35], but the physical picture there is very different. Those authors argue that quantum mechanics has operational meaning only under the existence of causal horizons because making probabilistic predictions requires decoherence with degrees of freedom outside the horizons. Our picture does not require such an extra agent to define probabilities (or quantum mechanics). The evolution of our $\Psi(t)$ is deterministic and unitary.

"premeasurement" situation for that experimenter, i.e.

$$P(\rho_\Lambda)\, d\rho_\Lambda = P(B|A), \quad \begin{cases} A: & \text{a particular "premeasurement" situation} \\ B: & \rho_\Lambda < \text{vacuum energy} < \rho_\Lambda + d\rho_\Lambda, \end{cases} \tag{12}$$

where $P(B|A)$ is defined in Eq. (10). Here, we have assumed that the number of SM vacua is sufficiently large for ρ_Λ to be treated as continuous in the range of interest. In general, the specification of the premeasurement situation can be arbitrarily precise; for example, we can consider a particular person taking a particular posture in a particular room, with the tip of the light cone used to define $|\Psi(t)\rangle$ located at a particular point in space. In practice, however, we are interested in the vacuum energy "a generic observer" will measure. We therefore need to relax the condition we impose as A; in other words, we need to "coarse grain" the premeasurement situation. In fact, some coarse graining is always necessary when we apply the formalism to postdiction (see discussions in Ref. [28]).

What condition A should we impose then? To address this issue, let us take the semi-classical picture of the framework, discussed in Section 2 of Ref. [28]. In this picture, the probability is given by

$$P(B|A) = \lim_{n\to\infty} \frac{\mathcal{N}_{A\cap B}}{\mathcal{N}_A}, \tag{13}$$

where $\mathcal{N}_A$ is the number of past light cones that satisfy A and are encountered by one of the n geodesics emanating from randomly distributed points on the initial hypersurface at $t = t_0$. (This is equivalent to Eq. (10) in the regime where the semi-classical picture is valid.) Since we vary only ρ_Λ, all the SM universes look essentially identical at early times when the vacuum energy is negligible. The assumed lack of statistical correlation between ρ_Λ and the multiverse dynamics then implies that we can consider a fixed number of geodesics emanating from a fixed *physical* volume at an early time (e.g. at reheating) in these universes, and see what fraction of these geodesics find the "premeasurement" situation A in each of these universes.

Given that we are focusing on the SM universes in which only the values of ρ_Λ are different, it is reasonable to expect that all the experimenters look essentially identical for different ρ_Λ, at least statistically—in particular, we assume that they have similar sizes, masses, and lifetimes. With this "coarse graining," the condition A can be taken, e.g., as: the geodesic intersects with the body of an experimenter at some time during their life. In practice, this makes the probability proportional to the fraction of a fixed comoving volume at an early time that later intersects with the body of an observer. Note that the details of the condition A here do not matter for the final results—for example, we can replace the "body" by "head" or "nose" without changing the results because its effect drops out from the normalized probability. Thus, in this situation (and any situation in which condition A can be formulated entirely in terms of things directly encountered by the geodesic), the semi-classical approximation to the scheme of Ref. [28] can be

calculated as the fat geodesic measure outlined in Ref. [37].[4] We emphasize that the consistent quantum mechanical solution to the measure problem in Ref. [28] *forces* this choice on us.

We can now present the formula for $P(\rho_\Lambda)$ in a more manageable form. Since the probability for one of the geodesics to intersect an experimenter is proportional to the number of experimenters and the density of geodesics, we have

$$P(\rho_\Lambda) \propto \sum_{a \in \text{habitable galaxies}} N_{\text{obs},a}\ \rho_{\text{geod},a}, \tag{14}$$

where $N_{\text{obs},a}$ and $\rho_{\text{geod},a}$ are, respectively, the *total* number of observers/experimenters and the density of geodesics in a "habitable" galaxy a. Here, we have approximated that $\rho_{\text{geod},a}$ is constant throughout the galaxy a. Note that since we count *intersections* of experimenters with geodesics, rather than just the number of observers (as in much previous work, e.g. [29]), our results differ from such previous results by our factor of $\rho_{\text{geod},a}$. Our remaining task, then, is to come up with a scheme that can "model" $N_{\text{obs},a}$ and $\rho_{\text{geod},a}$ reasonably well so that the final result is not far from the truth.

2.3 Approximating Observers

In this section, we convert Eq. (14) into an analytic expression that allows us to compute $P(\rho_\Lambda)$ numerically. We focus on presenting the basic logic behind our arguments. Detailed forms of the functions appearing below, e.g. $F(M,t)$ and $H(t';M,t)$, as well as useful fitting functions, are given in Appendix A.

Let us begin with $N_{\text{obs},a}$. We assume that, at a given time t, the number of observers arising in a given galaxy a is proportional to the total number of baryons in a

$$\frac{dN_{\text{obs},a}}{dt}(t) \propto N_{B,a}(t), \tag{15}$$

as long as stars are luminous. This assumption is reasonable if the rate of forming observers is sufficiently small, which appears to be the case in our universe. To estimate the number of baryons existing in galaxies, we use the standard Press-Schechter formalism [38], which provides the fraction of matter collapsed into halos of mass larger than M by time t, $F(M,t)$. Since the amount of baryons collapsed is proportional to that of matter, we can use this function F to estimate the number of observers and find[5]

$$P(\rho_\Lambda) \overset{?}{\propto} -\int dt \int dM\, \frac{dF(M,t)}{dM}\, \rho_{\text{geod}}(M,t). \tag{16}$$

[4] To our knowledge, no detailed study of the probability distribution of the cosmological constant according to the fat geodesic measure has been published prior to this work.

[5] Note that the sign of dF/dM is negative because of the definition of F.

The expression of Eq. (16) does not take into account the fact that forming intelligent observers takes time, or that observers appear only when stars are luminous (which we postulate, motivated by the assumption that we are typical observers). To include these effects, we use the extended Press-Schechter formalism [39], which gives the probability $H(t'; M, t)$ that a halo of mass M at time t virialized before t'. The probability density $P(\rho_\Lambda)$ can then be written as

$$P(\rho_\Lambda) \overset{?}{\propto} -\int dt \int dM \, \frac{dF(M,t)}{dM} \, \{H(t - t_{\rm evol}; M, t) - H(t - t_{\rm burn}; M, t)\} \, \rho_{\rm geod}(M, t), \tag{17}$$

where $t_{\rm evol}$ and $t_{\rm burn}$ are the time needed for intelligent observers to evolve and the characteristic lifetime of stars which limits the existence of life, respectively.

The density of geodesics $\rho_{\rm geod}(M, t)$ is proportional to that of a dark matter halo of mass M at time t, which is given by its average virial density:

$$\rho_{\rm geod}(M, t) \approx \left(\frac{dF(M, t_*)}{dM} \right)^{-1} \int_0^{t_*} dt' \, \rho_{\rm vir}(t') \, \frac{d^2F(M, t')}{dM dt'}, \tag{18}$$

where $t_* = \min\{t, t_{\rm stop}(M)\}$ with $t_{\rm stop}(M)$ the time after which the number of halos of mass M starts decreasing, i.e. when merging into larger structures dominates over formation of new halos: $d^2F/dMdt|_{t=t_{\rm stop}(M)} = 0$. (For the explicit expression of $\rho_{\rm vir}$, see Appendix A.) In the interest of speeding up numerical calculation, we approximate this by the virial density at the time when the rate of matter collapsing into a halo of mass M, i.e. $-d^2F/dMdt$, becomes maximum:

$$\rho_{\rm geod}(M, t) \approx \rho_{\rm vir}(\tau(M)) \, , \tag{19}$$

where $\tau(M)$ is given by

$$\left. \frac{d^3F(M,t)}{dMdt^2} \right|_{t=\tau(M)} = 0. \tag{20}$$

This approximation is indeed reasonable at the level of precision we are interested in: it works at the level of 20% for $t \gtrsim 1.7\tau(M)$ where the contribution to $P(\rho_\Lambda)$ almost entirely comes from.

Finally, there will be several additional anthropic conditions for a halo to be able to host intelligent observers. For example, the mass of a halo may have to be larger than some critical value $M_{\rm min}$ to efficiently form stars [40], and smaller than $M_{\rm max}$ for the galaxy to be cooled efficiently [41, 42]. Considering these factors, we finally obtain from Eqs. (17) and (19)

$$P(\rho_\Lambda) = -\frac{1}{N} \int_{t_{\rm evol}}^{t_{\rm f}} dt \int_{M_{\rm min}}^{M_{\rm max}} dM \, \frac{dF(M,t)}{dM} \, \{H(t - t_{\rm evol}; M, t) - H(t - t_{\rm burn}; M, t)\} \, \rho_{\rm vir}(\tau(M)) \, n(M, t), \tag{21}$$

where N is the normalization factor. Here,

$$t_{\rm f} = \begin{cases} \infty & \text{for } \rho_\Lambda \geq 0 \\ t_{\rm crunch} \equiv \sqrt{\frac{\pi}{6G_N|\rho_\Lambda|}} & \text{for } \rho_\Lambda < 0, \end{cases} \tag{22}$$

and we have put anthropic conditions besides $M_{\rm min,max}$ in the form of a function n. Note that F, H, and $\rho_{\rm vir}$ (and possibly n) all depend on the value of the vacuum energy ρ_Λ; see Appendix A.

In summary, $(dF/dM)\,(H|_{t-t_{\rm evol}} - H|_{t-t_{\rm burn}})\,n\,dMdt$ counts the (expected) number of observers in halos with mass between M and $M+dM$ at time between t and $t+dt$, and $\rho_{\rm vir}(\tau)$ is proportional to the density of geodesics in such a halo and time, and so Eq. (21) gives the probability by counting their intersections (as in Eq. (14)), with n implementing some anthropic conditions. One well-motivated origin for n is metallicity of stars, which affects the rate of planet formation (see e.g. Refs. [43, 44]). Here we simply model this effect by multiplying some power m of integrated star formation up to time $t - t_{\rm evol}$, which we assume to be proportional to the integrated galaxy formation rate for $M > M_{\rm min}$:

$$n(M,t) \propto \left(F(M_{\rm min}, \min\{t-t_{\rm evol}, \tilde{t}_{\rm stop}\}) - F(M, \min\{t-t_{\rm evol}, \tilde{t}_{\rm stop}\})\right)^m, \tag{23}$$

where $\tilde{t}_{\rm stop}$ is determined by $d\{F(M_{\rm min},t') - F(M,t')\}/dt'|_{t'=\tilde{t}_{\rm stop}} = 0$. (For the derivation of this expression, see Appendix B.) Motivated by the observation that the formation rate of certain (though not Earth-like) planets is proportional to the second power of host star metallicity [44], we consider the case $m=2$, as well as $m=1$.[6]

Another possible anthropic condition comes from the fact that if a halo is too dense, it may not host a habitable solar system because of the effects of close encounters [46]. Following Ref. [41], we assume this anthropic condition to take the form

$$n_\star \sigma_\dagger v_\dagger \lesssim \frac{1}{t_{\rm cr}}, \tag{24}$$

where $n_\star$, $\sigma_\dagger$, $v_\dagger$, and $t_{\rm cr}$ are the density of stars, critical "kill" cross section, relative velocity of encounters, and some timescale relevant for the condition. Since $n_\star \propto \rho_{\rm vir}$, $v_\dagger \sim v_{\rm vir} \propto M^{1/3}\rho_{\rm vir}^{1/6}$, and $\sigma_\dagger$ and $t_{\rm cr}$ are (expected to be) independent of M and $\rho_{\rm vir}$, this is translated into

$$n(M,t) = \Theta\left(\tilde{\rho}_{\rm max} - \rho_{\rm vir}(\tau(M))\left(\frac{M}{M_{\rm min}}\right)^{2/7}\right), \tag{25}$$

where $\Theta(x)$ is the step function ($=1$ for $x \geq 0$ and $=0$ for $x<0$), and we have normalized M by $M_{\rm min}$.

The value of $\tilde{\rho}_{\rm max}$ is highly uncertain. One way to estimate it is to follow Ref. [41] and take

$$n_\star \sim (1\ {\rm pc})^{-3}\left(\frac{\rho_{\rm vir}}{\rho_{\rm vir,MW}}\right), \quad \sigma_\dagger \sim \pi r_{\rm AU}^2, \quad v_\dagger \sim v_{\rm vir} \sim \sqrt{\frac{T_{\rm vir,MW}}{m_p}}\left(\frac{M}{M_{\rm MW}}\right)^{1/3}\left(\frac{\rho_{\rm vir}}{\rho_{\rm vir,MW}}\right)^{1/6}, \tag{26}$$

[6] There is observational data for metallicity of galaxies in our universe [45], which our crude model here does not reproduce quantitatively. However, when we straightforwardly extrapolate the empirical data to other universes, the same regions of the integrand in Eq. (21) are suppressed/enhanced so that the effect on our calculation is qualitatively the same. It must be noted, though, that the strength of the effect may change; e.g. $P(\rho_\Lambda)$ for our model with $m=1$ is qualitatively similar to the distribution obtained using the observation-motivated method with $m=3$.

where m_p is the proton mass, $r_{\rm AU} \simeq 1.5 \times 10^8$ km is the Sun-Earth distance, and $\rho_{\rm vir,MW} \sim 2 \times 10^{-26}$ g/cm^3, $T_{\rm vir,MW} \sim 5 \times 10^5$ K, and $M_{\rm MW} \sim 1 \times 10^{12} M_\odot$ are the virial density, virial temperature, and mass of the Milky Way galaxy, respectively. Using $t_{\rm cr} \sim t_{\rm evol} = 5$ Gyr, Eq. (24) leads to

$$\tilde{\rho}_{\rm max} \sim 9 \times 10^3 \, \rho_{\rm vir,MW} \Big(\frac{M_{\rm MW}}{M_{\rm min}} \Big)^{2/7} \sim 3 \times 10^{-22} \text{ g/cm}^3. \tag{27}$$

This corresponds to the constraint from direct encounters, i.e. the orbit of a planet being disrupted by the passage of a nearby star. There can also be a constraint from indirect encounters: a passing star perturbs an Oort cloud in the outer part of the solar system, triggering a lethal comet impact [41]. For a fixed M, this constraint can be about four orders of magnitude stronger than Eq. (27)

$$\tilde{\rho}_{\rm max} \sim 3 \times 10^{-26} \text{ g/cm}^3; \tag{28}$$

namely, our Milky Way galaxy may lie at the edge of allowed parameter space.

In our analysis below, we consider either or both of the above conditions Eqs. (23) and (25). In the real world, there are (almost certainly) more conditions needed for intelligent life to develop. However, incorporating these conditions would likely improve the prediction/postdiction for ρ_Λ. In this sense, our analysis may be viewed as a "conservative" assessment for the success of the framework, although it is still subject to uncertainties coming from the modeling of observers.

2.4 Distribution of the Cosmological Constant

Our modeling of observers has several parameters which need to be determined phenomenologically: Eq. (21) contains $M_{\rm min}$, $M_{\rm max}$, $t_{\rm evol}$, and $t_{\rm burn}$, while Eq. (25) contains $\tilde{\rho}_{\rm max}$. We take the "minimum" galaxy mass appearing in Eq. (21) to be

$$M_{\rm min} = 2 \times 10^{11} M_\odot, \tag{29}$$

below which the efficiency of star formation drops abruptly [40]. For $t_{\rm evol}$, and $t_{\rm burn}$, we take them approximately to be the age of the Earth and lifetime of the Sun, respectively:

$$t_{\rm evol} = 5 \text{ Gyr}, \qquad t_{\rm burn} = 10 \text{ Gyr}. \tag{30}$$

In our analysis below, we use Eqs. (29) and (30); we do not impose the constraint from galaxy cooling, i.e. we set $M_{\rm max} = \infty$. While the values of these parameters are highly uncertain, our results are not very sensitive to these values. The dependence of our results on them will be discussed at the end of this section. In Fig. 2, we present the normalized probability distribution for the vacuum energy $P(\rho_\Lambda)$ as a function of $\rho_\Lambda / \rho_{\Lambda,\rm obs}$, under several assumptions about the function n:

(i) "minimal" anthropic condition: $n(M, t) = 1$

	$P(\rho_\Lambda > 0)$	$P(\rho_\Lambda < 0)$
No condition	97%	3%
Metallicity, $m = 1$	87%	13%
Metallicity, $m = 2$	75%	25%
$\tilde{\rho}_{\rm max} = 6 \times 10^{-26}$ g/cm^3	92%	8%
$\tilde{\rho}_{\rm max} = 4.5 \times 10^{-26}$ g/cm^3	83%	17%
$\tilde{\rho}_{\rm max} = 3 \times 10^{-26}$ g/cm^3	63%	37%

Table 1: The probability of observing a positive and negative cosmological constant, $P(\rho_\Lambda > 0)$ and $P(\rho_\Lambda < 0)$, for six assumptions on the anthropic condition. In all cases, a positive value is preferred over a negative one, consistent with observation.

(ii) metallicity condition: Eq. (23) with $m = 1$ and 2

(iii) maximum virial density condition: Eq. (25) with $\tilde{\rho}_{\rm max} = \{3 \times 10^{-26},\ 4.5 \times 10^{-26},\ 6 \times 10^{-26}\}$ g/cm^3, which are $\{1, 1.5, 2\}$ times the value in Eq. (28).

(The result with $\tilde{\rho}_{\rm max}$ given by Eq. (27) is virtually identical to the case with the minimal anthropic condition.) The left panel presents the effects of metallicity, showing (i) and (ii), while the right panel those of $\tilde{\rho}_{\rm max}$, with (i) and (iii).

Interestingly, in all cases, our predictions prefer a positive cosmological constant over a negative one, as opposed to the situation in earlier measure proposals where strong preferences to negative values have been found [34]. In Table 1, we provide the probabilities of having $\rho_\Lambda > 0$ (and < 0) in all six anthropic scenarios. The absence of an unwanted preference towards negative ρ_Λ is satisfactory, especially given that the measure of Ref. [28] was not devised to cure this problem. It comes from the fact that the present measure does not have a large volume effect associated with the global geometry of anti-de Sitter space, which was responsible for a strong preference for negative ρ_Λ in earlier, geometric cutoff measures [34]. In contrast with these measures, the quantum measure of Ref. [28] does *not* count the number of events; rather, it gives *quantum mechanical weights* for "situations," i.e. quantum mechanical states as described from the viewpoint of a single observer (geodesic). The preference towards a positive value comes from the fact that for $\rho_\Lambda > 0$ some observers still form after vacuum energy domination, while for $\rho_\Lambda < 0$ it is not possible due to the big crunch.

Figure 2 shows that $P(\rho_\Lambda)$ is always peaked near $\rho_\Lambda = 0$, with the distribution becoming wider as the anthropic condition gets weaker. In Fig. 3, we plot the same distributions in logarithmic scale for $\rho_\Lambda/\rho_{\Lambda,\rm obs}$, limiting ourselves to $\rho_\Lambda > 0$. To show the probability density per tenfold, the vertical axis is chosen as $\rho_\Lambda P(\rho_\Lambda)/\rho_{\Lambda,\rm obs}$. From these figures, we find that our anthropic assumptions lead to results that are consistent with the observed value within one or two orders of magnitude. In particular, metallicity alone is enough to bring the agreement to

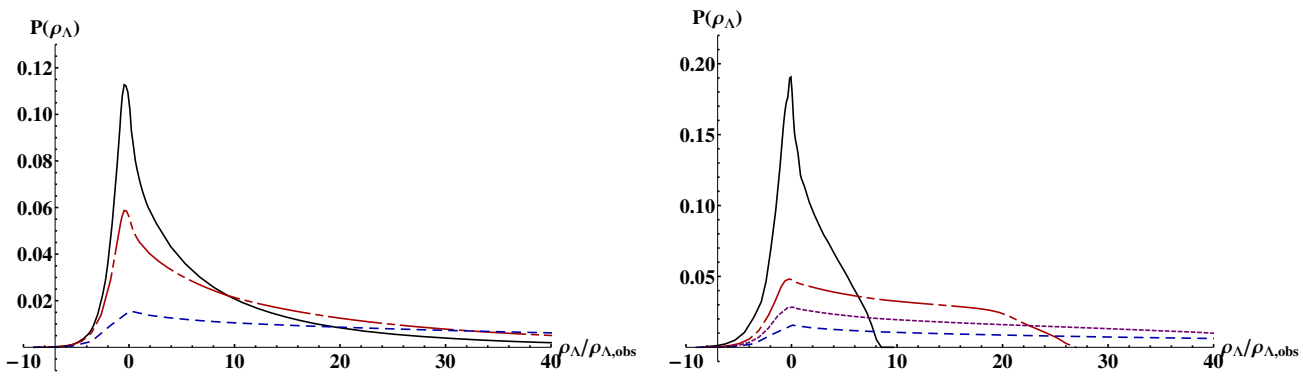

Figure 2: The normalized probability distribution of the vacuum energy $P(\rho_\Lambda)$ as a function of $\rho_\Lambda/\rho_{\Lambda,\mathrm{obs}}$. The left panel shows $P(\rho_\Lambda)$ with the metallicity condition, Eq. (23), with $m = 0$ (i.e. no condition; dashed, blue), $m = 1$ (dot-dashed, red), and $m = 2$ (solid, black). The right panel shows $P(\rho_\Lambda)$ with the upper bound $\tilde{\rho}_{\mathrm{max}}$, Eq. (25), with $\tilde{\rho}_{\mathrm{max}} = \infty$ (i.e. no constraint; dashed, blue), 6×10^{-26} g/cm^3 (dotted, purple), 4.5×10^{-26} g/cm^3 (dot-dashed, red), and 3×10^{-26} g/cm^3 (solid, black).

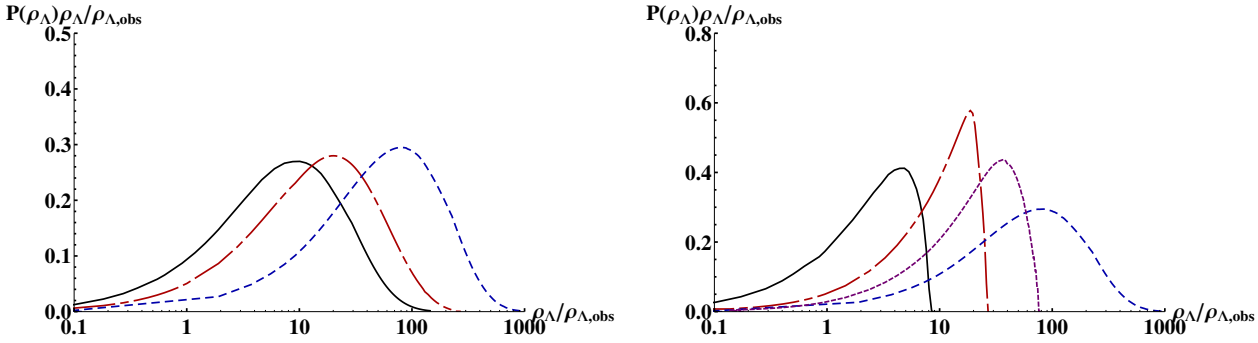

Figure 3: Same as Fig. 2, but the horizontal axis now in logarithmic scale. To show the probability density per tenfold, the vertical axis is chosen to be $\rho_\Lambda P(\rho_\Lambda)/\rho_{\Lambda,\mathrm{obs}}$. The distributions are normalized in the region $\rho_\Lambda > 0$.

an order of magnitude level. This is because mergers, which lead to an increase in metallicity, are suppressed for larger values of ρ_Λ due to earlier vacuum energy domination. This result is comfortable, especially given that the constraint from encounters is effective only if $\tilde{\rho}_{\mathrm{max}}$ is close to the Milky Way value, as in Eq. (28). Given our crude treatment of observers, we consider these results quite successful.

Finally, we discuss the sensitivity of our results to variations of M_{min}, M_{max}, t_{evol}, and t_{burn}, which can be thought of as "systematic effects" of our analysis. In Fig. 4, we show the distributions of $P(\rho_\Lambda)$ with the $m = 2$ metallicity constraint, varying the values of M_{min}, M_{max}, t_{evol}, and t_{burn}, respectively. We find that, while the detailed shape of $P(\rho_\Lambda)$ does change, our main conclusions are robust: (i) There is no strong preference to a negative vacuum energy; in fact, a

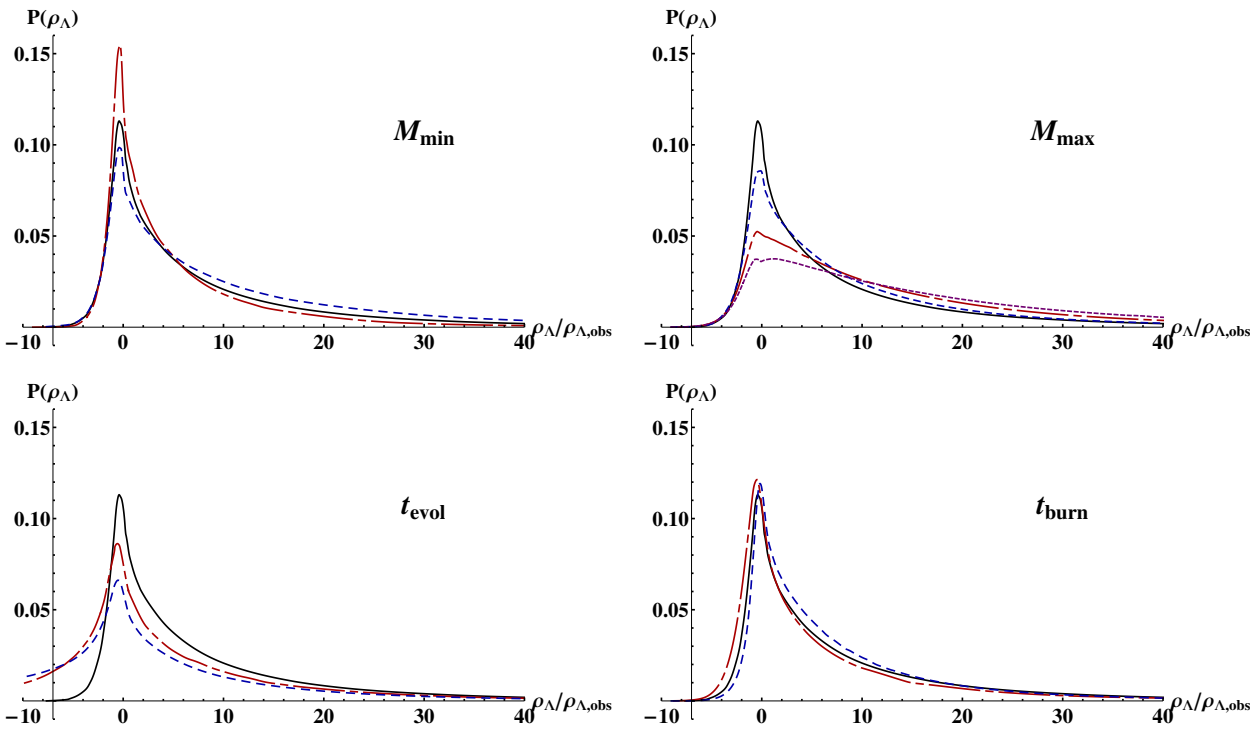

Figure 4: The normalized probability distribution $P(\rho_\Lambda)$ with the metallicity condition, Eq. (23), with $m = 2$. In the upper-left panel, $M_{\rm min}$ is varied as $2\times10^{11}M_\odot$ (solid, black), $6\times10^{11}M_\odot$ (dot-dashed, red), and $0.67\times10^{11}M_\odot$ (dashed, blue); and in the upper-right, $M_{\rm max}$ as ∞ (solid, black), $10^{14}M_\odot$ (dashed, blue), $10^{13}M_\odot$ (dot-dashed, red), and $2\times10^{12}M_\odot$ (dotted, purple). The lower left and right panels vary $t_{\rm evol}$ and $t_{\rm burn}$ as {(solid, black), (dot-dashed, red), (dashed, blue)} = $\{5, 1, 0\}$ Gyr and $\{10, 7, 15\}$ Gyr, respectively.

positive value is preferred. (ii) The predicted distribution of ρ_Λ is consistent with the observed value at an order of magnitude level with the metallicity constraint.

2.5 Conclusions

In this paper, we have studied the probability distribution of the cosmological constant (or the vacuum energy ρ_Λ) in the multiverse, using the quantum measure proposed in Ref. [28]. We have found that this measure does not lead to a strong preference for negative ρ_Λ, as opposed to earlier measures proposed based on geometric cutoffs, because it does not experience a large volume effect associated with the global geometry of anti-de Sitter space. Moreover, we have found that a positive value of ρ_Λ is preferred, consistent with observation.

We have found that a simple, intuitive condition based on metallicity is enough to reproduce the observed value of ρ_Λ at an order of magnitude level. This is comfortable because effects from other possible anthropic conditions, such as the ones from encounters, are much more sensitive

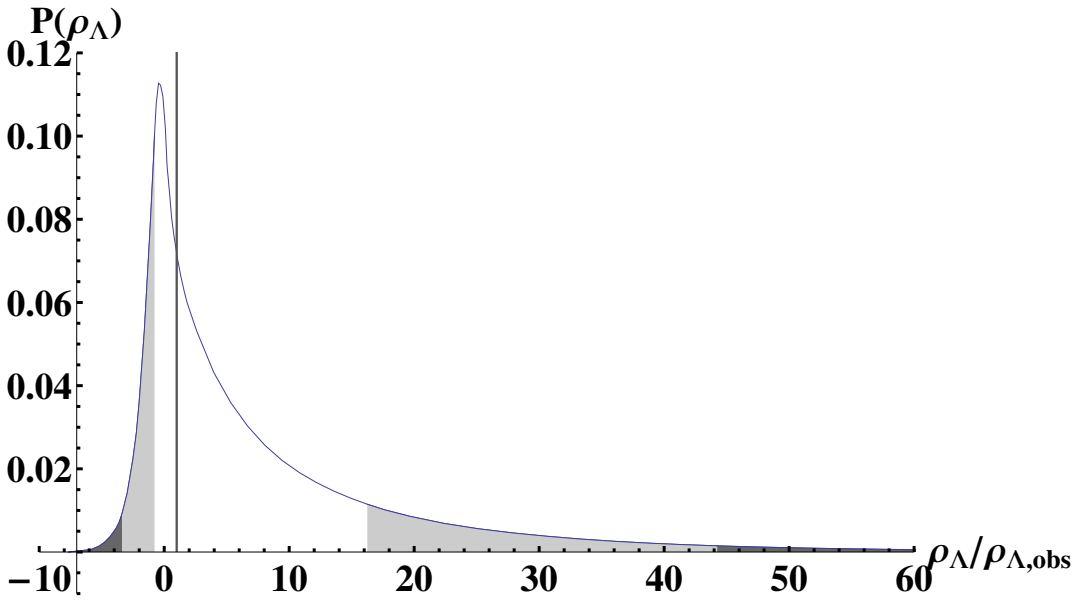

Figure 5: The normalized probability distribution $P(\rho_\Lambda)$ with a metallicity condition: Eq. (23) with $m = 2$. The light and dark shaded regions indicate those between 1 and 2σ, and outside 2σ, respectively. The observed value $\rho_\Lambda/\rho_{\Lambda,\text{obs}} = 1$ (denoted by a vertical line) is consistent with the distribution at the 1σ level.

to the details of the conditions. In Fig. 5, we present the normalized distribution $P(\rho_\Lambda)$ with the $m = 2$ metallicity constraint, where the 1 and 2σ regions are indicated. We find that the observed value is consistent with the calculated distribution at the 1σ level.

It would be interesting to refine our analysis including more detailed anthropic effects, such as those of star formation. Another possible extension of the analysis is to vary other cosmological parameters, such as the primordial density contrast Q and spatial curvature Ω_k (at a specified time), in addition to ρ_Λ. We plan to study these issues in the future.

3 Higgs Mass from D-Terms: a Litmus Test

3.1 Setup

We are interested in all $U(1)_X$ extensions of the MSSM consistent with a gauge invariant μ term. Mirroring [17, 20], we go to a convenient basis in which the charge parameters, g_X, p, and q, absorb all of the effects of kinetic and mass mixing between the $U(1)_X$ and $U(1)_Y$ gauge bosons above the electroweak scale. Thus, mixing only occurs after electroweak symmetry breaking, and the resulting effects are proportional to the Higgs vacuum expectation value (VEV). Of course, kinetic mixing is continually induced by running, so this choice of basis is renormalization scale dependent. However, this subtlety is largely irrelevant to our analysis,

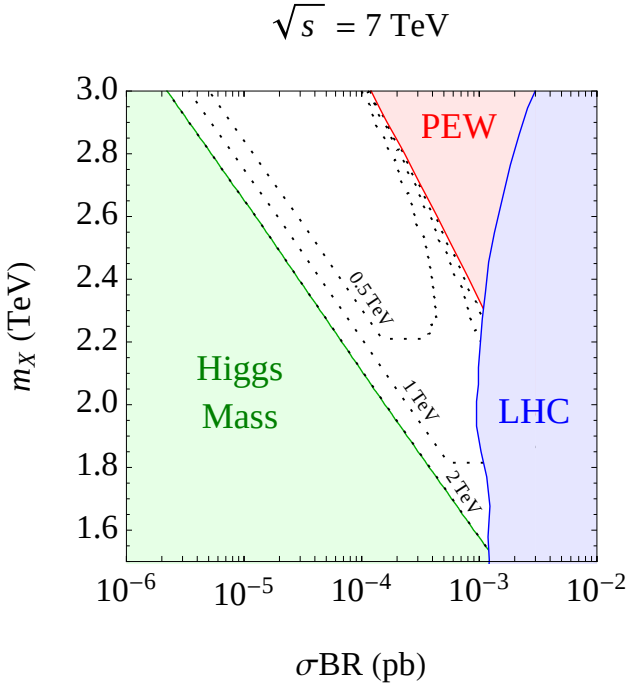

Figure 6: Litmus test: parameter space excluded by precision electroweak measurements (red), Higgs mass limits (green), and LHC resonance searches (blue) at $\sqrt{s} = 7$ TeV. For σBR too large, $g_X > g_{X,\max}$ yielding tension with precision electroweak and LHC constraints; for σBR too small, $g_X < g_{X,\min}$ yielding tension with $m_h \simeq 125$ GeV subject to the stop mass, shown here for $m_{\tilde{t}} = 0.5$ TeV, 1 TeV, 2 TeV. See the text in Sec. 3.2 for details.

which involves experimental limits in a relatively narrow window of energies around the weak scale. The advantage of this low energy parameterization is that it is very general and covers popular gauge extensions like $U(1)_B$, $U(1)_L$, $U(1)_{B-L}$, $U(1)_\chi$, and $U(1)_{3R}$. Furthermore, it is defined by a handful of parameters: m_X, g_X, p, and q.

Next, let us consider the issue of anomalies. If $p = q$, then according to Eq. (1) X is a linear combination of the Y and $B - L$, which is anomaly free if one includes a flavor triplet of right-handed neutrinos. If $p \neq q$ then the associated $B + L$ anomalies can be similarly cancelled by new particles. In general, these 'anomalons' can be quite heavy, in which case they can be ignored for our analysis.

We now examine the non-decoupling D-terms of $U(1)_X$ and their contribution to the Higgs potential. As we will see, these contributions are highly constrained by gauge symmetry and SUSY. To begin, consider a massive vector superfield composed of component fields

$$\{C, \chi, X, \lambda, D\}, \tag{31}$$

where X, λ, and D are the gauge field, gaugino, and auxiliary field, and C and χ are the

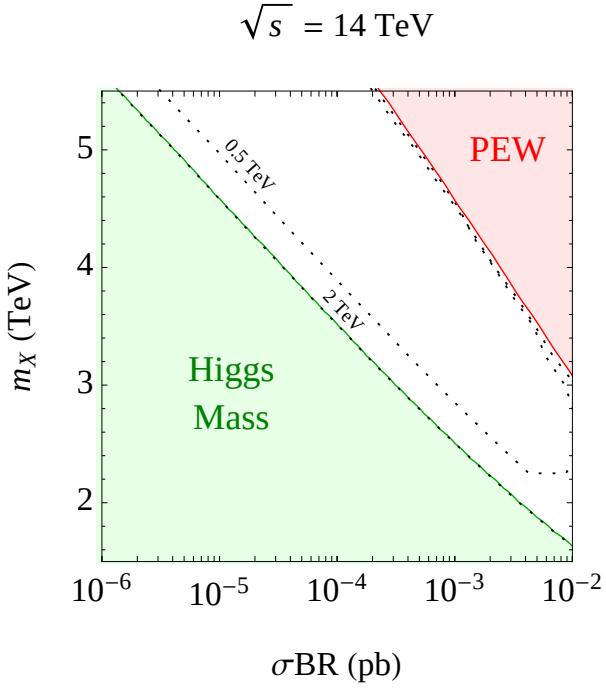

Figure 7: Same as Fig. 6 except with $\sqrt{s} = 14$ TeV, and stop mass contours $m_{\tilde{t}} = 0.5$ TeV, 2 TeV.

'longitudinal' modes eaten during the super-Higgs mechanism. Under SUSY transformations,

$$C \rightarrow C + i(\xi\chi - \bar{\xi}\bar{\chi}) \tag{32}$$

$$D \rightarrow D + \partial_\mu(-\xi\sigma^\mu\bar{\lambda} + \lambda\sigma^\mu\bar{\xi}). \tag{33}$$

Eq. (33) implies that $m\,C - D$ is a SUSY invariant on the equations of motion, $i\sigma^\mu\partial_\mu\bar{\lambda} = m\chi$, where $m = m_C = m_\lambda = m_X$ is the mass of the vector superfield.

On the other hand, the auxiliary field D can be re-expressed in terms of dynamically propagating fields by substituting the equations of motion. Since $m\,C - D$ is a SUSY invariant, this implies that

$$D = m\,C + D_{\rm IR} + D_{\rm UV} + \mathcal{O}(C^2), \tag{34}$$

where $D_{\rm IR}$ and $D_{\rm UV}$ label contributions from the (light) MSSM fields and the (heavy) $U(1)_X$ breaking fields, respectively, with all C dependence shown explicitly. The structure of Eq. (34) ensures that both the right and left hand sides transform the same under SUSY transformations. In the normalization of Eq. (1), $H_{u,d}$ has charge $\pm 1/2$ under $U(1)_X$, which implies

$$D_{\rm IR} = \frac{g_X}{2}(|H_u|^2 - |H_d|^2 + \ldots). \tag{35}$$

The effective potential for C and the MSSM scalars is obtained by setting all other fields to their

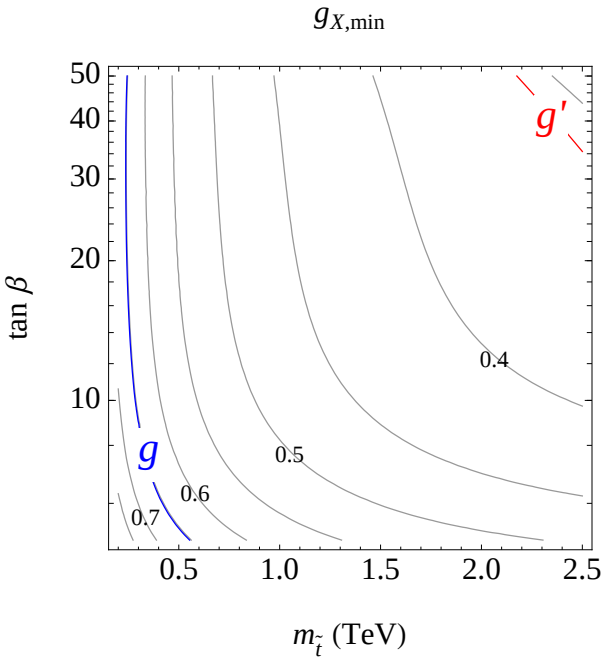

Figure 8: Contours of $g_{X,\min}$ which set the lower bound on g_X required to raise the Higgs mass to $m_h \simeq 125$ GeV. Values equal to the SM gauge couplings are highlighted.

VEVs, yielding

$$V = \frac{1}{2}D^2 + \frac{1}{2}\tilde{m}^2 C^2 + \tilde{t}C. \tag{36}$$

The first term is the usual SUSY D-term contribution, while the second and third terms arise from soft SUSY breaking effects such as non-zero F-terms. Here we have dropped terms $\mathcal{O}(C^3)$ and higher because they are unimportant for the Higgs quartic. Note that the spurions $\tilde{m}$ and $\tilde{t}$ depend implicitly on the VEVs of $U(1)_X$ breaking sector fields.

In the SUSY limit, $\tilde{m} = \tilde{t} = 0$ and integrating out C eliminates all $D_{\rm IR}$ dependence in the potential—no Higgs quartic is induced, as expected. If, on the other hand, $\tilde{t} \neq 0$, then C and $D_{\rm UV}$ will typically acquire messenger scale VEVs, yielding a huge tree-level contribution to m_{H_u} and m_{H_d} through a term linear in $D_{\rm IR}$. To avoid a destabilization of the electroweak scale, one usually assumes some ultraviolet symmetry, e.g. messenger parity, which ensures $\tilde{t} = 0$ and vanishing VEVs for C and $D_{\rm UV}$. We assume this to be the case here, in which case there is no D-term SUSY breaking.

On the other hand, SUSY breaking typically enters through $\tilde{m} \neq 0$, whose effects can be characterized by a simple SUSY spurion analysis. Let us model $\tilde{m}$ by an ultraviolet superfield spurion for F-term breaking, $\theta^2 F$. This spurion can effect the scalar sector in two ways: through the indirect shifts of scalar component VEVs, or through the direct couplings of $\theta^2 F$ to superfields. In the former, the masses of C and X may vary, but they do so together, and the states

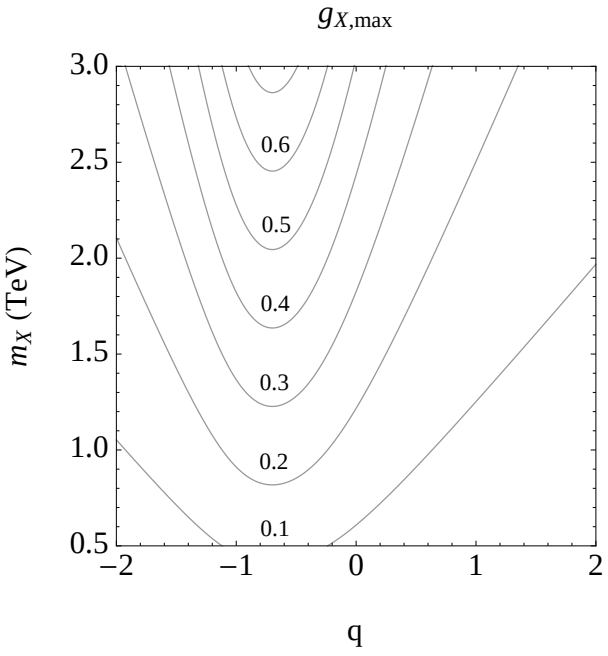

Figure 9: Contours of $g_{X,\max}$ which set the upper bound on g_X dictated by precision electroweak constraints. These limits depend primarily on the couplings of X to leptons, which are set by the q parameter.

remain degenerate. In the latter, only certain couplings are permitted between $\theta^2 F$ and the vector superfield components. Simple θ and $\bar{\theta}$ counting shows that X and D cannot couple directly to $\theta^2 F$, while C can. Hence, C is split in mass from the remainder of the gauge multiplet by F-term SUSY breaking.

Putting this all together, we rewrite Eq. (36) as

$$V = \frac{1}{2}\left(m_X C + D_{\rm IR}\right)^2 + \frac{1}{2}(m_C^2 - m_X^2)C^2, \tag{37}$$

where the coefficient of the second term is fixed so that m_C is the physical mass of C. Note that the prefactor for C in the first term is m_X—this can be verified by explicit computation, and is a direct consequence of the fact that X and D cannot couple directly to $\theta^2 F$. Integrating out C yields our final answer for the effective D-term contribution to the Higgs potential

$$V = \frac{1}{2}\varepsilon D_{\rm IR}^2 \tag{38}$$

$$\varepsilon = 1 - m_X^2/m_C^2, \tag{39}$$

which is a generalization of the specific examples in [9, 10]. In the SUSY limit, $m_C = m_X$ and the D-term contribution vanishes as expected. A positive contribution to the Higgs mass requires positive ε, which in turn requires that $m_C > m_X$. Importantly, $0 \leq \varepsilon < 1$ *independent of the ultraviolet completion*, which will be crucial later on when we derive model independent bounds.

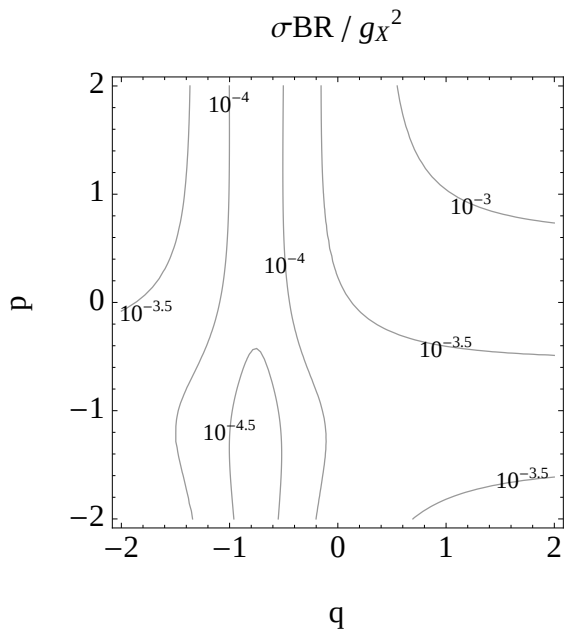

Figure 10: Contours of $\sigma \mathrm{BR}/g_X^2$ in pb for $m_X = 3$ TeV and $\sqrt{s} = 7$ TeV. Irrespective of the $U(1)_X$ charge parameters p and q, the rate is *always* non-zero.

3.2 Results

3.2.1 Experimental Constraints

In this section we analyze the experimental constraints on general $U(1)_X$ extensions of the MSSM. The relevant bounds come from the mass of the Higgs boson, precision electroweak measurements, and direct limits from the LHC.

• *Higgs Boson Mass.* Recent results from the LHC indicate hints of a SM-like Higgs boson at around $m_h \simeq 125$ GeV. Taken at face value, this imposes a stringent constraint on theories of $U(1)_X$ D-terms. In particular, combining Eq. (35) with Eq. (39) yields the mass of the Higgs boson

$$m_h^2 \;=\; m_Z^2 \cos^2 2\beta \left(1 + \frac{\varepsilon g_X^2}{g'^2 + g^2}\right) + \delta m_h^2, \tag{40}$$

where $0 \leq \varepsilon < 1$ independent of the ultraviolet completion. Here δm_h^2 denotes the usual radiative contributions to the Higgs mass in the MSSM,

$$\delta m_h^2 \;=\; \frac{3 m_t^4}{4\pi^2 v^2}\left(\log\frac{m_{\tilde{t}}^2}{m_t^2} + \frac{X_t^2}{m_{\tilde{t}}^2}\left(1 - \frac{X_t^2}{12 m_{\tilde{t}}^2}\right)\right), \tag{41}$$

where $m_{\tilde{t}} = (m_{\tilde{t}_1} m_{\tilde{t}_2})^{1/2}$ and $X_t = A_t - \mu \cot\beta$. In our actual analysis we employ the analytic expressions from [21] for the Higgs mass, which include two-loop leading log corrections.

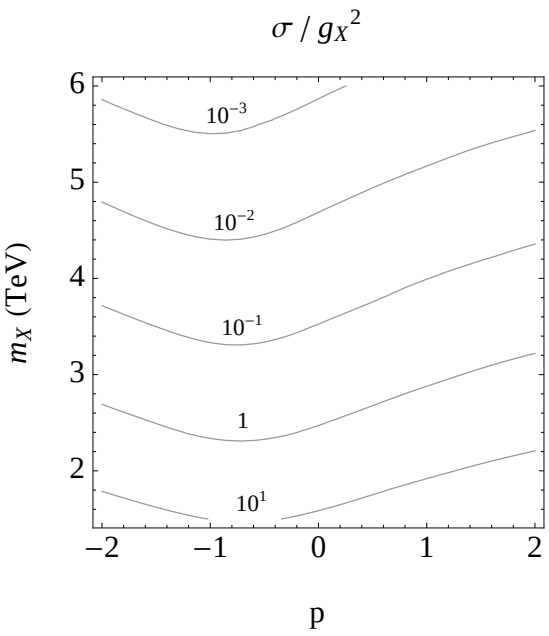

Figure 11: Contours of σ/g_X^2 in pb for $\sqrt{s} = 14$ TeV.

To simplify the parameter space, we take $A_t = 0$ and $\mu = 200$ GeV. Our results will be indicative of theories which have small A-terms, such as gauge mediated SUSY breaking. For a given value of $\tan\beta$ and $m_{\tilde{t}}$, the Higgs mass correction δm_h^2 is then fixed. Using Eq. (40) and $0 \leq \varepsilon < 1$, we find that g_X is bounded from below in order to accommodate $m_h \simeq 125$ GeV:

$$g_X > g_{X,\min}, \tag{42}$$

where $g_{X,\min}$ is a function of $(m_{\tilde{t}}, \tan\beta)$ shown in Fig. 8. For comparison, this figure includes contours of the SM electroweak gauge couplings, g' and g. At high $\tan\beta$, $U(1)_X$ is most effective at lifting the Higgs mass, so the stop masses can be the smallest. Note that in certain ultraviolet completions, ε can be quite small, in which case $g_{X,\min}$ and thus g_X will be much larger than the SM gauge couplings.

Lastly, let us comment briefly on the issue of fine tuning. In Sec. 3.1 we showed that non-decoupling D-terms require the scalar C to be split from the X boson at tree level. As a consequence, the low energy Higgs quartic coupling behaves like a hard breaking of SUSY and loops involving the components of the vector supermultiplet generate a quadratic divergence which is cut off by m_X. Since the Higgs fields are charged under $U(1)_X$, these radiative corrections contribute to the Higgs soft masses at one loop and can destabilize the electroweak hierarchy. In particular,

$$\delta m_{H_{u,d}}^2 \;=\; \frac{g_X^2}{64\pi^2} m_X^2 \log\left(\frac{m_X^6 m_C^2}{m_\lambda^8}\right), \tag{43}$$

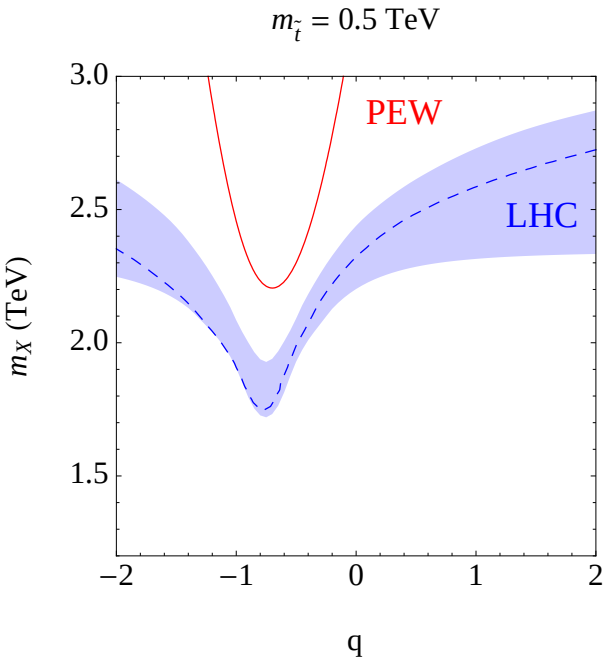

Figure 12: Limits from precision electroweak measurements (red solid), and LHC resonance searches for $p = q$ (blue dashed) and $p \neq q$ free (blue shaded), with $m_{\tilde{t}} = 0.5$ TeV, corresponding to $g_X > g_{X,\min} = 0.54$. Direct searches only exclude regions already disfavored by precision electroweak constraints.

which applies to R-symmetric limit [18, 19]. As required, when the components of the supermultiplet become degenerate, these corrections vanish. Due to the loop factor in Eq. (43) and the relative smallness of g_X required to lift the Higgs mass in Fig. 8, m_X can be quite large—even beyond LHC reach—without introducing fine-tuning more severe than $\sim 10\%$.

• *Precision Electroweak & Direct Limits.* Contributions to precision electroweak observables arise from two sources: mixing between the X and Z bosons, and couplings between the X boson and leptons. The former is always generated by electroweak symmetry breaking since the Higgs is, by construction, charged under $U(1)_X$. Meanwhile, the latter is also always present, since X has an irreducible coupling to leptons. Concretely, since $H_{u,d}$ has charge $\pm 1/2$, this implies that the composite operators QU^c, QD^c, and LE^c have charge $-1/2$, $+1/2$, and $+1/2$, respectively. As a result, X has an irreducible coupling to both leptons and quarks. The branching ratio to a single lepton flavor is:

$$\mathrm{BR}(X \to \ell\ell) \simeq \frac{5 + 12q + 8q^2}{66 + 24p + 24p^2 + 72q + 54q^2}, \tag{44}$$

where we have ignored kinematic factors and have assumed that the full MSSM field content can be produced in the decays of the X boson. This is a conservative choice because decoupling MSSM fields always increases $\mathrm{BR}(X \to \ell\ell)$, yielding more stringent constraints. For example, if X decays to the first and second generation squarks are kinematically forbidden, then $\mathrm{BR}(X \to$

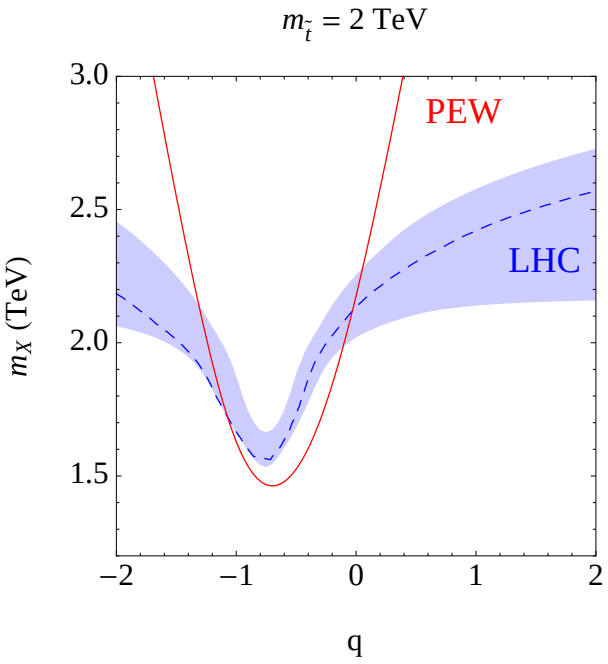

Figure 13: Same as Fig. 12, but for $m_{\tilde{t}} = 2$ TeV, corresponding to $g_X > g_{X,\min} = 0.36$.

$\ell\ell$) will increase at most by a factor of ~ 1.2. Using Eq. (44), we see that the leptonic branching ratio never vanishes for any finite values of p and q, and is strictly bounded from above at $\sim 15\%$.

Applying the methods of [22], we performed a precision electroweak fit on the theory parameters, g_X/m_X and q. For simplicity, we assumed a decoupling limit in which the lighter Higgs doublet drives the fit, so the Higgs sector is SM-like. As noted in [22], the resulting constraints are dominated by the couplings of X to leptons and the Higgs and are thus independent of p to a very good approximation. We have checked that our results match [20], which studies precision electroweak constraints on anomaly free $U(1)$ extensions. To accommodate 95% CL exclusion limits, the gauge coupling is bounded from above by

$$g_X < g_{X,\max}, \tag{45}$$

where $g_{X,\max}$ is a function of (q, m_X) shown in Fig. 9. Bounds are weakest near $q \simeq -0.7$ which is where the Y and L components of the X charge destructively interfere in a way that decreases the effective coupling of the X boson to leptons.

Lastly, for LHC resonance searches we are interested in the rate of resonant production, σBR for the process $pp \to X \to \ell\ell$. The leptonic branching ratios are given in Eq. (44) as a function of p and q, while the production cross-section of X bosons from proton collisions can be computed in terms of p with `MadGraph5`, including NNLO corrections from [23]. Remarkably, σBR is non-zero for any value of p and q, as shown in Fig. 10, which shows the rate normalized

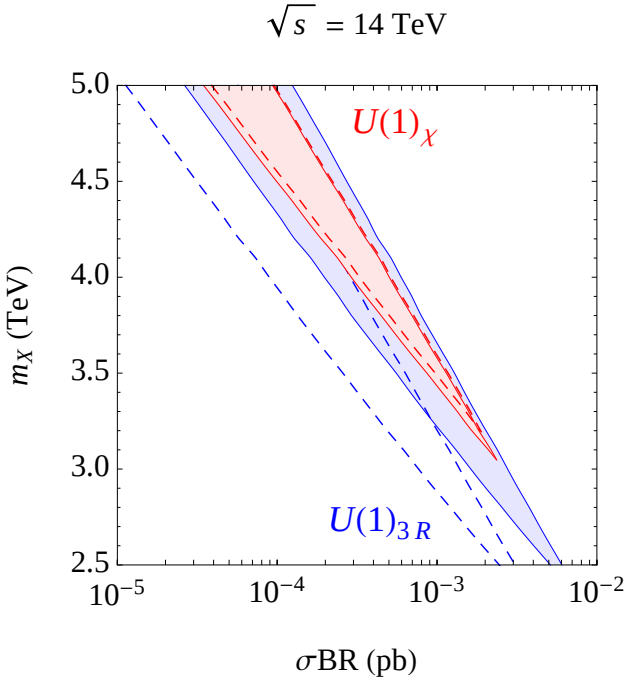

Figure 14: Allowed regions for $U(1)_\chi$ and $U(1)_{3R}$ for p and q fixed according to the exact GUT relations (solid shaded) or fixed to their values when running down from a high scale (dashed).

to g_X^2 for a sample parameter space point, $m_X = 3$ TeV at $\sqrt{s} = 7$ TeV. This crucially implies an irreducible rate for $pp \to X \to \ell\ell$, which we constrain with 5/fb results from the LHC [16]. For convenience, we also present the production cross-section normalized to g_X^2 in Fig. 11. By multiplying by BR($X \to \ell\ell$) from Eq. (44) and g_X^2 which is bounded from Figs. 8 and 9, one can determine a simple estimate for the future LHC reach for X bosons. At 100/fb and $\sqrt{s} = 14$ TeV, the LHC can reach as high as $m_X \sim 6$ TeV.

3.2.2 Litmus Tests

The experimental constraints enumerated in Sec. 3.2.1 provide stringent and complementary limits on the allowed parameter space of $U(1)_X$ theories. We can now combine these bounds in order to identify various 'litmus tests' for non-decoupling D-terms.

To begin, consider Figs. 12 and 13, which depict experimentally excluded regions in the (q, m_X) plane for $m_{\tilde{t}} = 0.5$ TeV, 2 TeV, respectively. The region below the solid red line is excluded by precision electroweak measurements. This limit is to good approximation independent of p, which controls the coupling of X to quarks. The region below the blue dashed line is excluded by LHC resonance searches in the anomaly free case, i.e. $p = q$. Allowing $p \neq q$ to vary freely then floats the boundary of this exclusion within the blue shaded region.

For stop masses in the natural window, $m_{\tilde{t}} \lesssim 500$ GeV, these plots imply that the LHC

has not excluded any region of parameter space which was not already disfavored by precision electroweak limits. Conversely, if natural SUSY employs non-decoupling D-terms, then the LHC should not yet have seen any signs of the X boson. Given precision electroweak measurements, $m_X \gtrsim 2.2$ TeV for natural SUSY. For heavier stop masses, Fig. 13 shows that the LHC has covered some but not very much new ground.

Let us now discuss Figs. 6 and 7. At fixed values of the masses, m_X and $m_{\tilde{t}}$, we can scan over the charge parameters, g_X, p, and q, discarding any model points which are in conflict with precision electroweak and Higgs limits. By this procedure, we obtain an 'image' of the viable theory space on the observable space, $(\sigma\text{BR}, m_X)$. Each dotted black contour in Figs. 6 and 7 depicts a maximal allowed region in $(\sigma\text{BR}, m_X)$ obtained via this scan for a given stop mass. Any theory of natural SUSY which employs non-decoupling D-terms predicts an X boson residing somewhere within the region corresponding to $m_{\tilde{t}} = 0.5$ TeV. Since we have marginalized over g_X, p, and q, these exclusions are model independent.

The allowed regions in Figs. 6 and 7 are bounded at small and large σBR because $g_{X,\text{min}} < g_X < g_{X,\text{max}}$, where $g_{X,\text{min}}$ is a function of $(m_{\tilde{t}}, \tan\beta)$ and $g_{X,\text{max}}$ is a function of (q, m_X). As described in Sec. 3.2.1, the lower bound arises from the requirement that non-decoupling D-terms sufficiently lift the Higgs mass up to $m_h \simeq 125$ GeV, while the upper bound arises from precision electroweak constraints. Since the production cross-section of X bosons depends on g_X, one can translate this allowed window in g_X into an allowed window in rate, $\sigma\text{BR}_{\text{min}} < \sigma\text{BR} < \sigma\text{BR}_{\text{max}}$.

Because Figs. 6 and 7 were derived from a parameter scan, model points near the Higgs boundary limit versus those near the precision electroweak boundary limit correspond to different values of p and q. This results in different precision electroweak constraints for different stop masses—an effect that is amplified on the near flat direction in $m_{\tilde{t}}$ that traverses diagonally across the plot.

Note that the values of $\sigma\text{BR}_{\text{min}}$ depicted in Figs. 6 and 7 are conservative—they coincide with the parameter choice $\varepsilon = 1$ in Eq. (39). Because this corresponds to $m_C \to \infty$, this choice is rather unphysical. In general, $\varepsilon < 1$, in which case $\sigma\text{BR}_{\text{min}}$ will be substantially larger and the allowed region will shrink.

Also, at a fixed value of σBR, increasing m_X makes precision electroweak bounds more severe, which is unintuitive from the point of view of decoupling. However, this occurs because in order to keep σBR constant with increasing m_X, the coupling g_X must increase even faster, inducing tension with precision electroweak measurements.

Alternatively, we can fix p and q rather than marginalize with respect to them. GUT relations provide a natural choice for the values of p and q:

$$U(1)_\chi \;:\; p = q = -5/4 \tag{46}$$

$$U(1)_{3R} \;:\; p = q = -1/2. \tag{47}$$

However, running from high scales can induce kinetic mixing which offsets p and q, which are intrinsically low energy parameters. For $m_{\rm GUT} \simeq 2 \times 10^{16}$ GeV, this can shift $p = q$ up to about -1.2 for $U(1)_\chi$ and down to about -0.8 for $U(1)_{3R}$, although the precise numbers depend on the GUT scale and matter content [20]. Because GUT values may be preferred from a top down viewpoint, we present the allowed regions for these theories at $\sqrt{s} = 14$ TeV in Fig. 14, depicted as the colored wedges. As before, lower values of σBR are excluded by the Higgs mass results (where here we have fixed $m_{\tilde{t}} = 0.5$ TeV) while higher values of σBR are excluded by precision electroweak constraints. Theories corresponding to the exact GUT values for $p = q$ in Eq. (47) are depicted by solid lines, while the dashed lines depict values of $p = q$ including running from high scales. For both $U(1)_\chi$ and $U(1)_{3R}$, a narrow allowed region is prescribed, outside of which is either unnatural or experimentally excluded.

3.3 Conclusions

In this paper we have analyzed a broad class of $U(1)_X$ extensions of the MSSM in which $m_h \simeq 125$ GeV is accommodated by non-decoupling D-terms. We have assumed that $U(1)_X$ is flavor universal and allows a gauge invariant μ term, but impose no additional theoretical constraints.

Our main result is a simple litmus test for this class of theories at the LHC—if non-decoupling D-terms are instrumental in lifting the Higgs mass, then experimental constraints imply that an X boson can only be observed in the allowed region depicted in Figs. 6 and 7. Crucially, for natural SUSY this region is bounded from below in σBR for $pp \to X \to \ell\ell$, so we should expect an irreducible level of X boson production at the LHC. Our check is very model independent, since our input constraints have been marginalized over all charge assignments for $U(1)_X$. Furthermore, general arguments from SUSY and gauge invariance dictate the very particular form for non-decoupling D-terms shown Eq. (39), so our results are also independent of the ultraviolet details of $U(1)_X$ breaking. We have also presented an analogous litmus test which can be applied for the specific GUT inspired models described in Fig. 14.

4 Supersymmetry with Light Stops

4.1 Formulation in Warped Space

4.1.1 The basic structure

In this section we present a class of models realizing the basic setup of Fig. 1. We formulate it in a 5D warped spacetime with the extra dimension y compactified on an S^1/Z_2 orbifold: $0 \leq y \leq \pi R$. The spacetime metric is given by

$$ds^2 = e^{-2ky} \eta_{\mu\nu} dx^\mu dx^\nu + dy^2, \tag{48}$$

where k is the AdS curvature, which is taken to be somewhat (typically a factor of a few) smaller than the 5D cutoff scale M_*. The 4D Planck scale, $M_{\rm Pl}$, is given by $M_{\rm Pl}^2 \simeq M_5^3/k$, where M_5 is the 5D Planck scale, and we take $k \sim M_* \sim M_5 \sim M_{\rm Pl}$. For now, we take the size of the extra dimension R to be a free parameter, satisfying $kR \gtrsim 1$. If we choose $kR \sim 10$, the TeV scale is generated by the AdS warp factor: $k' \equiv ke^{-\pi kR} \sim$ TeV [68].

We consider that the SM gauge supermultiplets $\{V_A, \Sigma_A\}$ $(A = 1, 2, 3)$ as well as matter supermultiplets $\{\Psi_i, \Psi_i^c\}$ ($\Psi = Q, U, D, L, E$ with $i = 1, 2, 3$ the generation index) propagate in the 5D bulk. (Here, we have used the 4D $N = 1$ superfield notation; see e.g. [69].) Assuming the boundary conditions

$$\begin{pmatrix} V_A(+,+) \\ \Sigma_A(-,-) \end{pmatrix}, \qquad \begin{pmatrix} \Psi_i(+,+) \\ \Psi_i^c(-,-) \end{pmatrix}, \tag{49}$$

the low-energy field content below the Kaluza-Klein (KK) excitation scale $\sim k'$ is the gauge and matter fields of the Minimal Supersymmetric Standard Model (MSSM). They arise from the zero modes of V_A and Ψ_i.

Now, suppose the supersymmetry breaking chiral superfield X is localized on the ultraviolet (UV) brane at $y = 0$, while two Higgs-doublet chiral superfields H_u and H_d are on the infrared (IR) brane at $y = \pi R$. Then the bulk matter and gauge fields can interact with these fields through

$$\mathcal{L} = \delta(y)\left[\int d^4\theta \sum_\Psi \left\{\hat{\eta}_{ij}^\Psi X^\dagger X \Psi_i^\dagger \Psi_j + \left(\hat{\zeta}_{ij}^\Psi X \Psi_i^\dagger \Psi_j + \text{h.c.}\right)\right\} + \sum_A \left\{\int d^2\theta\, \hat{\xi}_A X \mathcal{W}_A^\alpha \mathcal{W}_{A\alpha} + \text{h.c.}\right\}\right] \tag{50}$$

and

$$\mathcal{L} = \delta(y - \pi R)\, e^{-3\pi kR} \int d^2\theta \left(\hat{y}_{ij}^u Q_i U_j H_u + \hat{y}_{ij}^d Q_i D_j H_d + \hat{y}_{ij}^e L_i E_j H_d\right) + \text{h.c.}, \tag{51}$$

respectively, where $\mathcal{W}_{A\alpha}$ are the field-strength superfields.[7]

In addition, we can introduce a singlet field S either in the bulk or on the $y = \pi R$ brane with interactions

$$\begin{aligned} \mathcal{L} \;=\; & \delta(y - \pi R)\, e^{-3\pi kR} \left\{\int d^2\theta \left(\hat{\lambda} S H_u H_d + \hat{f}(S)\right) + \text{h.c.}\right\} \\ & + \delta(y) \int d^4\theta \left\{\hat{\eta}^S X^\dagger X S^\dagger S + \left(\hat{\zeta}^S X S^\dagger S + \text{h.c.}\right)\right\}, \end{aligned} \tag{52}$$

where $\hat{f}(S)$ is a holomorphic function of S, and the terms in the second line exist only if S is the bulk field, $\{S, S^c\}$. The introduction of S allows us to accommodate a relatively heavy Higgs boson, including $m_h = 125$ GeV.

[7] We adopt the definition of the delta function $\int_0^\varepsilon \delta(y) = \int_{\pi R - \varepsilon}^{\pi R} \delta(y - \pi R) = 1$, where $0 < \varepsilon < \pi R$.

The Lagrangian for the free part of a bulk supermultiplet $\{\Phi, \Phi^c\}$ is given by

$$\begin{aligned}\mathcal{L} &= e^{-2ky}\int d^4\theta\,(\Phi^\dagger\Phi + \Phi^c\Phi^{c\dagger}) + e^{-3ky}\left\{\int d^2\theta\,\Phi^c\Big(\partial_y + M_\Phi - \frac{3}{2}k\Big)\Phi + \text{h.c.}\right\} \\ &\quad + \delta(y)\int d^4\theta\, z_\Phi \Phi^\dagger\Phi, \end{aligned} \tag{53}$$

where we have included a UV-brane localized kinetic term z_Φ (> 0), which plays an important role in our discussion. (A possible IR-brane localized kinetic term is irrelevant for the discussion.) There are two parameters in this Lagrangian: M_Φ and z_Φ. The parameter M_Φ controls the wavefunction profile of the zero mode in the bulk. For $M_\Phi > k/2$ ($< k/2$) the wavefunction of a zero mode arising from Φ is localized to the UV (IR) brane; for $M_\Phi = k/2$ it is flat (see e.g. [70]). The parameter z_Φ is important for a field with $M_\Phi \gtrsim k/2$; it controls how much of the zero mode is regarded as the brane and bulk degrees of freedom. For $z_\Phi M_\Phi \gg 1$, the zero mode is mostly brane field-like, while for $z_\Phi M_\Phi \ll 1$ it is bulk field-like.

Our setup is realized by taking $M_\Phi \gtrsim k/2$ and $z_\Phi M_\Phi \gg 1$ for the first two generations of matter while $M_\Phi \ll k/2$ for the third generation quark-doublet and right-handed top multiplets $\{Q_3, Q_3^c\}$ and $\{U_3, U_3^c\}$. This implies that the former are mostly brane field-like, while the latter are bulk fields with the wavefunctions localized to the IR brane. (In the 4D interpretation discussed in Section 4.1.3, these correspond to mostly elementary and composite fields, respectively.) The zero-mode wavefunctions for the other third generation multiplets $\{D_3, D_3^c\}$, $\{L_3, L_3^c\}$, and $\{E_3, E_3^c\}$ are more flexible, although they are still subject to constraints from flavor physics, both to reproduce realistic Yukawa matrices and to avoid excessive supersymmetric contributions to flavor violation.

More specifically, the wavefunction of the zero mode of the $\{\Phi, \Phi^c\}$ multiplet in Eq. (53) is given by

$$f_\Phi(y) = \frac{1}{\sqrt{z_\Phi + \frac{1}{2(M_\Phi - \frac{k}{2})}(1 - e^{-2\pi R(M_\Phi - \frac{k}{2})})}}\, e^{-(M_\Phi - \frac{k}{2})y} \tag{54}$$

in the "conformal-field" basis, in which 5D scalar and fermion fields ϕ and ψ are rescaled from the original component fields in Φ as $\phi = e^{-ky}\Phi|_0$ and $\psi_\alpha = e^{-ky}\Phi|_\theta$. The low-energy 4D theory below $\sim k'$ is obtained by integrating over y with this wavefunction. For the superpotential terms, it leads to

$$\mathcal{L}_{\text{4D}} = \int d^2\theta\,\big(y^u_{ij} Q_i U_j H_u + y^d_{ij} Q_i D_j H_d + y^e_{ij} L_i E_j H_d + \lambda S H_u H_d + f(S)\big) + \text{h.c.}, \tag{55}$$

where the 4D coupling constants (quantities without hat) are related with the 5D ones (with hat) by

$$y^u_{ij} = \hat{y}^u_{ij}\, x_{Q_i} x_{U_j}, \qquad y^d_{ij} = \hat{y}^d_{ij}\, x_{Q_i} x_{D_j}, \qquad y^e_{ij} = \hat{y}^e_{ij}\, x_{L_i} x_{E_j}, \qquad \lambda = \hat{\lambda}\, x_S, \tag{56}$$

and $f(S) = \hat{f}(x_S S)$. Here, the factors x_Φ ($\Phi = Q_i, U_i, D_i, L_i, E_i, S$) are given by

$$x_\Phi \equiv f_\Phi(\pi R) \simeq \begin{cases} \frac{1}{\sqrt{z_\Phi + \frac{1}{2M_\Phi}}}\, e^{-\pi R M_\Phi} & \text{for } M_\Phi \gg \frac{k}{2} \\ \frac{1}{\sqrt{z_\Phi + \pi R}} & \text{for } M_\Phi \sim \frac{k}{2} \\ \sqrt{2(\frac{k}{2} - M_\Phi)} & \text{for } M_\Phi \ll \frac{k}{2} \end{cases}, \tag{57}$$

where we have used $z_\Phi k e^{-\pi k R} \ll 1$ for $M_\Phi \ll k/2$, which is satisfied in the relevant parameter region considered later.[8] The case with brane S is obtained by replacing x_S with 1.

For the supersymmetry-breaking terms, the 4D theory below $\sim k'$ yields

$$\begin{aligned} \mathcal{L}_{\rm 4D} \;=\; & \int d^4\theta \Big\{ \sum_\Psi \eta^\Psi_{ij} X^\dagger X \Psi_i^\dagger \Psi_j + \eta^S X^\dagger X S^\dagger S + \big(\sum_\Psi \zeta^\Psi_{ij} X \Psi_i^\dagger \Psi_j + \zeta^S X S^\dagger S + \text{h.c.} \big) \Big\} \\ & + \sum_A \Big\{ \int d^2\theta\, \xi_A X \mathcal{W}_A^\alpha \mathcal{W}_{A\alpha} + \text{h.c.} \Big\}, \end{aligned} \tag{58}$$

where

$$\eta^\Psi_{ij} = \hat{\eta}^\Psi_{ij}\, r_{\Psi_i} r_{\Psi_j}, \qquad \eta^S = \hat{\eta}^S\, r_S^2, \qquad \zeta^\Psi_{ij} = \hat{\zeta}^\Psi_{ij}\, r_{\Psi_i} r_{\Psi_j}, \qquad \zeta^S = \hat{\zeta}^S\, r_S^2, \qquad \xi_A = \hat{\xi}_A, \tag{59}$$

and the factors r_Φ are given by

$$r_\Phi \equiv f_\Phi(0) \simeq \begin{cases} \frac{1}{\sqrt{z_\Phi + \frac{1}{2M_\Phi}}} & \text{for } M_\Phi \gg \frac{k}{2} \\ \frac{1}{\sqrt{z_\Phi + \pi R}} & \text{for } M_\Phi \sim \frac{k}{2} \\ \sqrt{2(\frac{k}{2} - M_\Phi)}\, e^{-\pi R(\frac{k}{2} - M_\Phi)} & \text{for } M_\Phi \ll \frac{k}{2} \end{cases}. \tag{60}$$

The case with brane S is obtained by $r_S \to 0$.

As will be discussed in Section 4.1.3, the models presented here can be interpreted, through the AdS/CFT correspondence, as those of composite Higgs-top in the supersymmetric desert. As such, small neutrino masses can be generated by the conventional seesaw mechanism. Specifically, we can introduce right-handed neutrino supermultiplets $\{N_i, N_i^c\}$ in the bulk, with Majorana masses and neutrino Yukawa couplings located on the UV and IR branes, respectively:

$$\mathcal{L} = \delta(y) \int d^2\theta\, \frac{\hat{M}_{ij}}{2} N_i N_j + \delta(y - \pi R)\, e^{-3\pi k R} \int d^2\theta\, \hat{y}^\nu_{ij} L_i N_j H_u + \text{h.c.} \tag{61}$$

For $M_{N_i} \sim k/2$, this naturally generates small neutrino masses of the observed size (assuming the absence of tree-level neutrino-mass operators such as $\int d^2\theta\, (L H_u)^2$ on the IR brane) [71]. Alternatively, small Dirac neutrino masses can be obtained if we prohibit the Majorana masses for N_i and localize them to the UV brane [72].

[8] The expression $M_\Phi \ll k/2$ here and after means that $|M_\Phi| \ll k/2$ or $M_\Phi < 0$.

4.1.2 Physics of flavor—fermions and sfermions

We now discuss the flavor structure of quarks/leptons and squarks/sleptons in more detail. Suppose that all the couplings on the UV brane are roughly of $O(1)$ in units of some messenger scale $M_{\rm mess}$. In this case, Eqs. (59, 60) imply that the zero modes localized to the IR brane obtain only exponentially suppressed supersymmetry-breaking masses (at scale k'):

$$m_{\tilde{Q}_3,\tilde{U}_3}/m_{\tilde{\Psi}_{1,2}} \ll 1. \tag{62}$$

A main motivation to consider light stops is naturalness, Eq. (5). To keep this, we take $m_{\tilde{Q}_3,\tilde{U}_3} \lesssim$ (400 – 500) GeV (after evolving down to the weak scale). In order to satisfy constraints from flavor violation, the right-handed bottom and first two generation squark masses should be in the multi-TeV region [57, 73]. We therefore choose $M_{D_3} \gtrsim k/2$, and

$$m_{\tilde{\Psi}_{1,2}} \sim m_{\tilde{b}_R} \sim \text{a few TeV}, \tag{63}$$

$$m_{\tilde{t}_L,\tilde{t}_R} \sim m_{\tilde{b}_L} \lesssim (400 - 500)\ \text{GeV}. \tag{64}$$

The masses of $\tilde{L}_3$ and $\tilde{E}_3$ are less constrained, although we consider $M_{L_3,E_3} \gtrsim k/2$ in most of the paper, leading to $m_{\tilde{\tau}_L,\tilde{\tau}_R,\tilde{\nu}_\tau} \sim$ a few TeV. With the mass splitting of Eqs. (63, 64), the hypercharge D-term contribution does not have a large effect on the Higgs mass-squared parameter to destabilize naturalness.

The masses of the gauginos are determined by parameters such as $\hat{\xi}_A$, $\hat{\eta}^\Psi_{ij}$ and z_Φ, which depend on a detailed mechanism generating operators in Eq. (50). Motivated by naturalness, in this paper we take

$$m_{\tilde{B},\tilde{W}} \lesssim 1\ \text{TeV}, \quad m_{\tilde{g}} \sim 1\ \text{TeV}. \tag{65}$$

The gluino mass, $m_{\tilde{g}} \simeq M_3$, is chosen so that the stops do not obtain large radiative corrections exceeding Eq. (64), and that the theory is not excluded by the LHC data: $m_{\tilde{g}} \gtrsim 700$ GeV [58]. The above equations (63 – 65) specify the superpartner spectra we consider.[9]

What about the flavor structure for quarks/leptons and those among the first two generation sfermions? In this paper, we consider a theory in which all the nontrivial flavor structures are generated from physics of the bulk (and on the IR brane). In the 4D "dual" picture discussed in Section 4.1.3, this corresponds to the setup in which the nontrivial flavor structure is generated through interactions of the elementary sector with the strongly-interacting composite sector. This implies that all the flavor violating effects are shut off in the high energy limit, giving the conditions

$$\hat{\eta}^\Psi_{ij} \propto \hat{\zeta}^\Psi_{ij} \propto (z_\Psi)_{ij} \tag{66}$$

[9] In deriving these expressions, we have ignored possible contributions to the supersymmetry breaking masses from the sector that stabilizes the radius of the extra dimension. This assumption is justified for certain ways of stabilizing the radius; see, e.g., Ref. [64].

in flavor space, $i, j = 1, 2, 3$. In particular, in the field basis that $(z_\Psi)_{ij} \propto \delta_{ij}$, which we can always take, $\hat{\eta}^\Psi_{ij} \propto \hat{\zeta}^\Psi_{ij} \propto \delta_{ij}$. This can be achieved if the operators in Eq. (50) are generated by flavor universal dynamics, e.g. gauge mediation on the UV brane.

With the multi-TeV masses, the spectrum of the first two generation sfermions must be somewhat degenerate, to avoid stringent constraints from flavor. From Eq. (60), we find that the first two generation sfermion masses depend on $\hat{\eta}^\Psi_{ij}$, $(z_\Psi)_{ij}$, and $(M_\Psi)_{ij}$. (Note that we take the bulk masses larger than $k/2$ for the first two generations of matter.) In the field basis that $\hat{\eta}^\Psi_{ij}$ and $(z_\Psi)_{ij}$ are proportional to the unit matrix, $\hat{\eta}^\Psi_{ij} \equiv \hat{\eta}^\Psi \delta_{ij}$ and $(z_\Psi)_{ij} \equiv z_\Psi \delta_{ij}$, the only source of flavor violation comes from $(M_\Psi)_{ij}$, which we can diagonalize by field rotation in flavor space: $(M_\Psi)_{ij} = M_{\Psi_i} \delta_{ij}$. The effects of flavor violation are then of order

$$\frac{\Delta \tilde{m}_{ij}}{\tilde{m}_i + \tilde{m}_j} = \frac{r_{\Psi_i} - r_{\Psi_j}}{r_{\Psi_i} + r_{\Psi_j}}, \tag{67}$$

multiplied by appropriate flavor mixing angles arising from diagonalization of the 4D Yukawa matrices. Here, r_{Ψ_i} are given in Eq. (60). Requiring that these effects satisfy constraints from the K-$\bar{K}$ physics [74], we find, for example,

$$z_\Psi k \gtrsim \{15, 12, 4\} \quad \text{for } \tilde{m} = \{1, 4, 10\} \text{ TeV}, \tag{68}$$

for $M_{\Psi_2}/k \simeq 0.6$ and $M_{\Psi_1}/k \simeq 0.7$, which produces hierarchy of $O(0.1)$ by the difference of wavefunction profiles between Ψ_1 and Ψ_2. Here, $\tilde{m}$ represents the masses of the first two generation sfermions, and we have assumed the maximal phase in the relevant matrix element. While the precise constraint on z_Ψ depends on detailed modeling of flavor, we generically need nonvanishing $z_\Psi \gtrsim O(10/k)$ in the case of the maximal phase in K-$\bar{K}$ mixing.[10]

The structure of the 4D Yukawa couplings can be read off from Eqs. (56, 57). For a field with $M_\Phi > k/2$, we have a suppression arising from the wavefunction profile of the zero mode, $\epsilon_\Phi \equiv e^{-\pi R(M_\Phi - k/2)}$, contributing to the hierarchy of the Yukawa couplings [70, 75]. In addition, fields with $M_{\Psi_{1,2}} \gtrsim k/2$ may have an additional suppression $\epsilon \equiv 1/\sqrt{z_\Phi M_*}$ if $z_\Phi k \gg 1$. For example, if we take $M_{D_3, L_3, E_3} \gtrsim k/2$, then we find

$$y_u \propto \begin{pmatrix} \epsilon^2 \epsilon_{Q_1} \epsilon_{U_1} & \epsilon^2 \epsilon_{Q_1} \epsilon_{U_2} & \epsilon\, \epsilon_{Q_1} \\ \epsilon^2 \epsilon_{Q_2} \epsilon_{U_1} & \epsilon^2 \epsilon_{Q_2} \epsilon_{U_2} & \epsilon\, \epsilon_{Q_2} \\ \epsilon\, \epsilon_{U_1} & \epsilon\, \epsilon_{U_2} & 1 \end{pmatrix}, \qquad y_d \propto \begin{pmatrix} \epsilon^2 \epsilon_{Q_1} \epsilon_{D_1} & \epsilon^2 \epsilon_{Q_1} \epsilon_{D_2} & \epsilon^2 \epsilon_{Q_1} \epsilon_{D_3} \\ \epsilon^2 \epsilon_{Q_2} \epsilon_{D_1} & \epsilon^2 \epsilon_{Q_2} \epsilon_{D_2} & \epsilon^2 \epsilon_{Q_2} \epsilon_{D_3} \\ \epsilon\, \epsilon_{D_1} & \epsilon\, \epsilon_{D_2} & \epsilon\, \epsilon_{D_3} \end{pmatrix}, \tag{69}$$

$$y_e \propto \begin{pmatrix} \epsilon^2 \epsilon_{L_1} \epsilon_{E_1} & \epsilon^2 \epsilon_{L_1} \epsilon_{E_2} & \epsilon^2 \epsilon_{L_1} \epsilon_{E_3} \\ \epsilon^2 \epsilon_{L_2} \epsilon_{E_1} & \epsilon^2 \epsilon_{L_2} \epsilon_{E_2} & \epsilon^2 \epsilon_{L_2} \epsilon_{E_3} \\ \epsilon^2 \epsilon_{L_3} \epsilon_{E_1} & \epsilon^2 \epsilon_{L_3} \epsilon_{E_2} & \epsilon^2 \epsilon_{L_3} \epsilon_{E_3} \end{pmatrix}, \tag{70}$$

[10] In the 4D picture of Section 4.1.3, this corresponds to the case where the first two generations of matter are mostly elementary, with the contributions of the strong sector to their kinetic terms suppressed compared to those at tree level.

where $O(1)$ factors are omitted in each element, and $\epsilon_\Phi \ll 1$ only if $\pi R(M_\Phi - k/2) \gg 1$ and $\epsilon \ll 1$ only if $z_\Phi k \gg 1$. Therefore, with suitable choices for M_{Ψ_i}, the observed pattern of the Yukawa couplings can be reproduced through physics of the bulk (i.e. the dynamics of the strong sector in the 4D picture) while keeping approximate flavor universality for the first two generation sfermion masses.

4.1.3 4D interpretation

Models discussed here can be interpreted as purely 4D models formulated in the conventional grand desert, using the AdS/CFT correspondence. (For discussions on this correspondence, see e.g. [59, 76].) In the 4D picture, the first two generations of matter are (mostly) elementary, while the third generation quark-doublet and right-handed top multiplets arise as composite fields of some strongly interacting sector, which exhibits nontrivial dynamics at an exponentially small scale $\approx k' = ke^{-\pi kR}$. (We mostly consider that the right-handed bottom and third-generation lepton multiplets are elementary, although there is some flexibility on this choice.) This strong dynamics also produces S, H_u, and H_d fields, together with superpotential interactions $W_H = \lambda S H_u H_d + f(S)$ at k'. (We focus on the case of IR-brane localized S in this section.) Since the Higgs-top sector is strongly coupled at k', the Landau pole constraint for the couplings in W_H (and the top Yukawa coupling) needs to be satisfied only below k' [61], realizing the λSUSY framework in Ref. [77].

Supersymmetry breaking is mediated at the scale $M_{\rm mess}$, giving TeV to multi-TeV masses to the elementary sfermions as well as the gauginos. The effect of supersymmetry breaking in the composite sector is diluted by the near-conformal strong dynamics [62], as long as operators associated with this effect have large anomalous dimensions [63]. This therefore yields only negligible soft masses for the composite fields at k'.[11] A composite field, however, may obtain sizable supersymmetry breaking masses (only) if it mixes with an elementary state, which in the 5D picture corresponds to delocalizing the state from the IR brane.

The top Yukawa coupling is naturally large as the relevant fields are all composite. On the other hand, the Yukawa couplings for the first two generations of matter are generated through mixing of these states with fields in the composite sector, so are suppressed. The amount of suppression depends on the dimension of the mixing operator, and thus varies field by field, yielding a hierarchical pattern for the Yukawa matrices. Note that this way of dynamically generating the Yukawa hierarchy does not contradict the stringent constraints on supersymmetric flavor violation as long as supersymmetry breaking mediation at $M_{\rm mess}$ is flavor universal (e.g.

[11] In our models, supersymmetry breaking masses in the elementary sector, $\tilde{m} \sim$ a few TeV, is smaller than the compositeness scale, $k' \gtrsim 10$ TeV (see below). Therefore, the problem of a potentially large D-term operator [63], intrinsic to the framework of Refs. [62, 63, 64], does not arise, unless this operator is generated directly by the physics at $M_{\rm mess}$. The dilution of supersymmetry breaking effects in the composite sector has been studied explicitly in Ref. [65] in a setup similar to ours, using Seiberg duality.

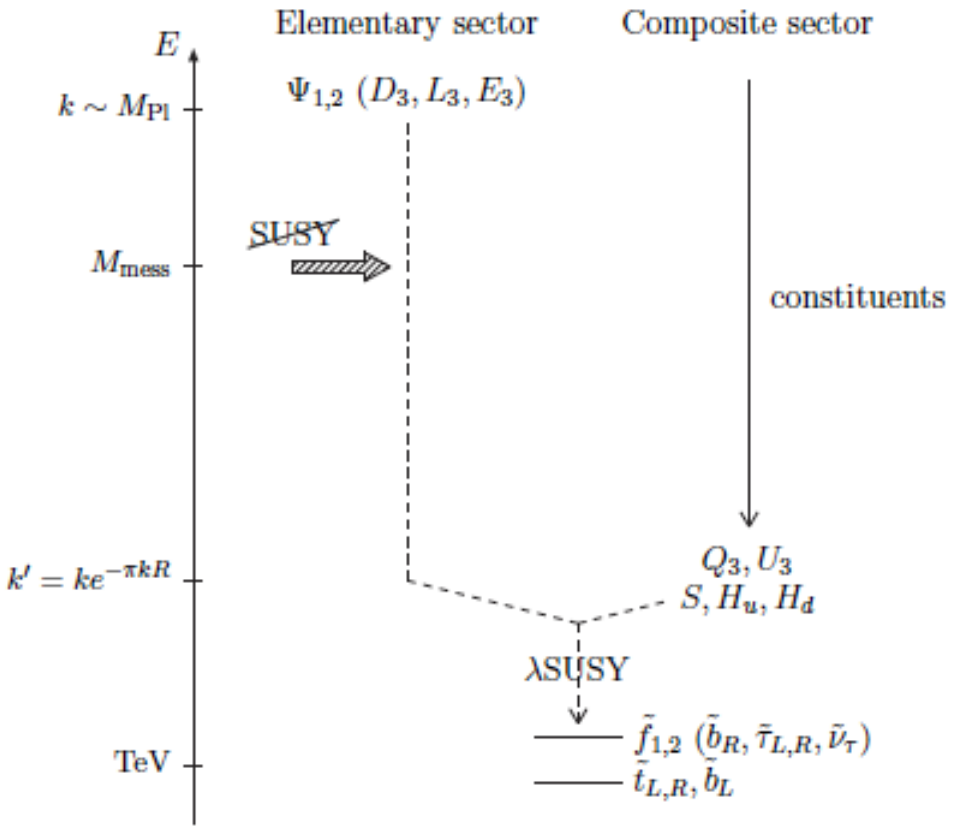

Figure 15: The 4D interpretation of the models. The first two generations of matter are elementary, while the Higgs and top multiplets arise as composite states at the scale of strong dynamics, k'. The theory between k' and TeV is λSUSY in Ref. [77] (with a modest Higgs-sector coupling λ), with light stops and left-handed sbottom.

as in the case of gauge mediation) *and* the contribution to the kinetic terms of the elementary fields from the strong sector is small (which corresponds to the condition in Eq. (68) in 5D). The overall picture for the 4D interpretation described here is depicted schematically in Fig. 15.

The value of the compositeness scale k' is constrained by phenomenological considerations. As in Eq. (64), we take the stops light to keep electroweak symmetry breaking natural. On the other hand, the LHC bound on the gluino mass for these values of stop masses is $m_{\tilde{g}} \gtrsim 700$ GeV, so that we need a little "hierarchy" between $m_{\tilde{t}}$ and $m_{\tilde{g}}$. Since $m_{\tilde{t}}$ receives a positive contribution from $m_{\tilde{g}}$ through renormalization group evolution, this bounds the scale k' from above. The precise bound is (exponentially) sensitive to the low energy parameters, but we typically find that k' must be below an intermediate scale; in particular, it cannot be at the unification scale. The value of k' is also limited from above by Landau pole considerations for the couplings in W_H.

The lower bound on k' can be obtained for a fixed $m_{\tilde{g}}$ by requiring that $\tilde{t}_L$, $\tilde{t}_R$, and $\tilde{b}_L$ are sufficiently heavy to avoid the LHC bounds. Assuming that these states decay either into the lightest neutralino or the gravitino within the detector, which we would need anyway to avoid a strong constraint on quasi-stable stops, the masses of $\tilde{t}_L$ and $\tilde{b}_L$ must be larger than about 250 GeV [58]. Moreover, if the neutralino to which these states decay is lighter than ≈ 100 GeV (or if they decay into the gravitino), then the mass of $\tilde{b}_L$ must be larger than about 400 GeV [78]. Since the running masses for these states, $m_{\tilde{Q}_3}$ and $m_{\tilde{U}_3}$, are vanishing at k' (up to small threshold corrections), this limits k' from below for a fixed $m_{\tilde{g}}$. In this paper, we take

$$k' \gtrsim 10 \text{ TeV}, \tag{71}$$

so that the theory below the compositeness scale is the supersymmetric standard model with the superpartner spectrum given by Eqs. (63 – 65). With these values of k', other lower bounds on k' coming from precision electroweak measurements and flavor/CP violation induced by KK excitations are satisfied [79]. (Note that the masses of the lowest KK excitations are given by $\approx \pi k'$.)

Our models have the supersymmetric grand desert between k' and $k \sim M_{\rm Pl}$. Thus, if the strong sector respects a (global) unified symmetry, then we can discuss gauge coupling unification, along the lines of Ref. [80]. The prediction depends on the location of matter fields, especially D_3, L_3 and E_3; in the minimal case where these fields have $M_\Phi \gtrsim k/2$, the three SM gauge couplings approach at $\sim 10^{17}$ GeV, but with the precision of unification worse than that in the SM ($\delta g^2/\bar{g}^2 \approx 15\%$ at the unification scale). We do not pursue the issue of unification further in this paper.

4.2 Electroweak Symmetry Breaking

4.3 Overview

As outlined in Section 4.1.3, our theory above the compositeness scale k' is $SU(3)_C \otimes SU(2)_L \otimes U(1)_Y$ gauge theory that has the elementary fields $\Psi_{1,2}$ (and D_3, L_3, E_3) and the strongly interacting near-conformal sector. The beta functions for the gauge group are given by

$$b_A = b_A^{\rm MSSM} - b_A^{Q_3+U_3+H_{u,d}} + b_{\rm CFT}, \tag{72}$$

where $b_{\rm CFT}$ is the contribution from the strong sector, which corresponds to $1/g_{\rm 5D}^2 k$ in the 5D picture, and is universal if this sector respects a (global) unified symmetry. Supersymmetry breaking masses for the elementary fields, including the gaugino masses M_A, are generated at $M_{\rm mess}$, and they are evolved down to k' by the renormalization group equations with Eq. (72). The composite fields appear at k', which have vanishing supersymmetry breaking masses at that scale (up to small threshold corrections of $O(M_A^2/16\pi^2)$ in squared masses).

Physics of electroweak symmetry breaking is governed by the dynamics of the composite sector and the gaugino masses. At scale k', the strong sector produces the superpotential

$$W_H = \lambda S H_u H_d + f(S) + \cdots , \tag{73}$$

for the Higgs sector, where the dots represent higher dimension terms which are generically suppressed by the warped-down cutoff scale $M_*' = M_* e^{-\pi k R}$. In case M_*' is close to the TeV scale, these higher dimension terms could affect phenomenology; for example, the term $(H_u H_d)^2$ can contribute to the Higgs boson mass [81]. Similarly, higher dimension terms in the Kähler potential may affect phenomenology; for example, the terms $S^\dagger H_u H_d$ and $S^\dagger H_u^\dagger Q D$ can lead to a μ term and down-type quark masses if S has an F-term expectation value.

In general, for relatively large values of k' envisioned in Eq. (71), the effects of these higher dimension operators are insignificant, except possibly for light quark/lepton masses. We therefore consider only renormalizable terms in the Higgs potential. In particular, in the rest of the paper we focus on the case where W_H contains only dimensionless terms in 4D, and discuss how electroweak symmetry breaking can work in our models. In doing so, we assume

$$m_{\tilde{Q}_3, \tilde{U}_3, H_u, H_d} \approx 0, \tag{74}$$

at k', i.e. we ignore possible threshold corrections at that scale, which are highly model-dependent. (We later consider dynamics at the IR scale in which non-vanishing m_S^2 is generated at k' to reproduce correct electroweak symmetry breaking.) This will illustrate basic features of electroweak symmetry breaking in our framework, in the minimal setup.

4.3.1 Higgs sector: κSUSY

We consider a variant on the λSUSY model [77], which has the superpotential of the Next-to-Minimal Supersymmetric Standard Model (NMSSM) form:

$$W_H = \lambda S H_u H_d + \frac{\kappa}{3} S^3. \tag{75}$$

To distinguish from other λSUSY studies in which the κ term does not play a dominant role, we call this model κSUSY. We assume that S, H_u, and H_d are all localized to the IR brane, so we require λ and κ to be perturbative only up to the scale k', which we take to be 10 – 1000 TeV. For $k' = 10$ TeV, for example, we obtain $\lambda(M_Z) \lesssim 1.8$ for $\kappa(M_Z) = 0.7$; for $k' = 1000$ TeV, $\lambda(M_Z) \lesssim 1.1$ for $\kappa(M_Z) = 0.7$.

Because of Eq. (74), the only relevant dimensionful parameters for electroweak symmetry breaking are the gaugino masses, except possibly for the supersymmetry breaking mass for the S field (which we will introduce in the next subsection). They set the scale for the soft

supersymmetry breaking masses in the scalar potential

$$\begin{aligned} V &= |\lambda H_u H_d + \kappa S^2|^2 + |\lambda S H_u|^2 + |\lambda S H_d|^2 \\ &\quad + m_S^2|S|^2 + m_{H_u}^2|H_u|^2 + m_{H_d}^2|H_d|^2 + (\lambda A_\lambda S H_u H_d - \frac{\kappa}{3} A_\kappa S^3 + \text{h.c.}) \\ &\quad + \frac{g^2}{8}(H_u^\dagger \sigma^a H_u + H_d^\dagger \sigma^a H_d)^2 + \frac{g'^2}{8}(|H_u|^2 - |H_d|^2)^2, \end{aligned} \tag{76}$$

through renormalization group evolution below k'. Successful electroweak symmetry breaking requires all the S, H_u, and H_d fields to obtain vacuum expectation values, $v_s \equiv \langle S \rangle$, $v_u \equiv \langle H_u \rangle$, and $v_d \equiv \langle H_d \rangle$.

Once the singlet has a vacuum expectation value, v_s, we obtain $\mu = \lambda v_s$ and $B_\mu = \lambda A_\lambda v_s + \kappa \lambda v_s^2 = \mu(A_\lambda + \kappa\mu/\lambda)$, where B_μ is the holomorphic supersymmetry breaking Higgs mass-squared. We thus obtain the following Higgs mass-squared matrix (in the h_u-h_d-s basis):

$$\mathcal{M}^2_{\text{scalar}} \equiv \tfrac{1}{2}\tfrac{\partial^2 V}{\partial v_i \partial v_j} = \tfrac{1}{2}\left(\tfrac{\partial^2 V}{\partial v_i \partial v_j} - \delta_{ij}\tfrac{1}{v_i}\tfrac{\partial V}{\partial v_i}\right) = \tfrac{1}{2}\times$$

$$\begin{pmatrix} \bar{g}^2 v_u^2 + \frac{2B_\mu}{\tan\beta} & (4\lambda^2 - \bar{g}^2) v_u v_d - 2B_\mu & 4\mu v_u\left(\lambda - \frac{\kappa}{\tan\beta} - \frac{\lambda A_\lambda}{2\mu \tan\beta}\right) \\ (4\lambda^2 - \bar{g}^2) v_u v_d - 2B_\mu & \bar{g}^2 v_d^2 + 2B_\mu \tan\beta & 4\mu v_d\left(\lambda - \kappa \tan\beta - \frac{\lambda A_\lambda \tan\beta}{2\mu}\right) \\ 4\mu v_u\left(\lambda - \frac{\kappa}{\tan\beta} - \frac{\lambda A_\lambda}{2\mu \tan\beta}\right) & 4\mu v_d\left(\lambda - \kappa \tan\beta - \frac{\lambda A_\lambda \tan\beta}{2\mu}\right) & \frac{8\kappa B_\mu}{\lambda}\left(1 - \frac{\mu\left(A_\lambda + \frac{A_\kappa}{4}\right)}{B_\mu} + \frac{\lambda^3 A_\lambda v_u v_d}{4\kappa\mu B_\mu}\right) \end{pmatrix}, \tag{77}$$

where $\bar{g}^2 \equiv g^2 + g'^2$, and we have assumed that all three expectation values are real and nonzero. For us, the A_λ and A_κ terms are small because they are generated essentially only through weak renormalization group evolution below k'; $|A_{\lambda,\kappa}| \lesssim O(10\text{ GeV})$. Other than contributing to B_μ, they also contribute to singlet-doublet mixing and pseudoscalar masses, but we will ignore them in the following discussion on the (non-pseudo)scalar spectrum, as the result is not very sensitive to the values of such small A terms.

We now discuss important differences between κSUSY and the MSSM as well as previous λSUSY/NMSSM studies [52, 82, 83]. They are illustrated in Fig. 16, where (tree-level) scalar masses are plotted as a function of λ for sample values of $\tan\beta, \kappa, \mu$.

- We see that κ plays a crucial role in this theory because it appears in $B_\mu \supset \kappa\mu^2/\lambda$. It determines the degree of decoupling of the SM-like Higgs from the heavier scalars. The limit $\kappa = 0$ leads to nearly massless modes and is therefore unacceptable. In fact, as we shall see, we need $\kappa \sim \lambda$ for a successful theory of electroweak symmetry breaking.

- The new quartic term $\lambda^2|H_u H_d|^2$ leads to an extra doublet-doublet mixing which competes against B_μ: $\mathcal{M}^2_{12} = (2\lambda^2 - \bar{g}^2/2) v_u v_d - B_\mu$. As long as $2\lambda^2 v_u v_d < B_\mu + \bar{g}^2 v_u v_d/2$, this leads to the well-known enhancement of the Higgs mass in λSUSY, see Eq. (78). However, once

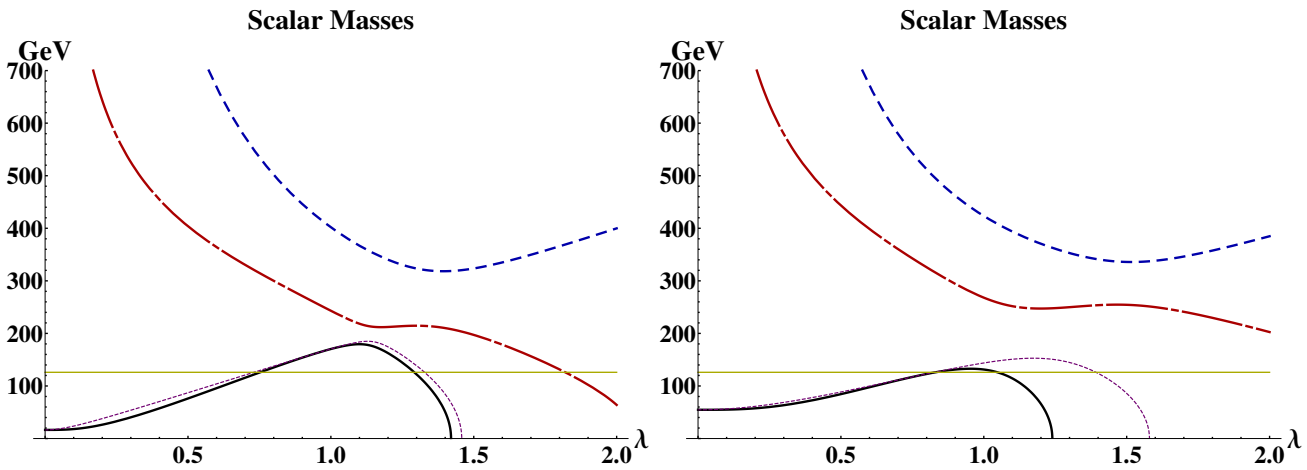

(a) $\tan\beta = 1.2$, $\kappa = 1.0$, $\mu = 200$ GeV (b) $\tan\beta = 2.0$, $\kappa = 1.0$, $\mu = 200$ GeV

Figure 16: Two representative plots of the scalar mass spectrum in κSUSY. The solid (black), dot-dashed (red), and dashed (blue) lines represent the masses of the three mass eigenstates, which at small λ correspond to the SM, heavy-doublet, and singlet like Higgs bosons, respectively. The horizontal (yellow) line shows $m_h = 125$ GeV, and the dotted (violet) line is the mass of the lightest Higgs boson with singlet-doublet mixing turned off by hand. In the left figure we see that λ-doublet mixing is responsible for lowering the mass of the Higgs below its decoupling limit, Eq. (78), rather than doublet-singlet mixing. This is a generic feature for $\tan\beta \sim 1$. In the right figure, we see that as we increase $\tan\beta$, singlet-doublet mixing sets in at lower λ than doublet-doublet mixing but that both are important in lowering the Higgs mass below Eq. (78).

$2\lambda^2 v_u v_d > B_\mu + \bar{g}^2 v_u v_d/2$, the absolute magnitude of the off-diagonal term now increases with λ which leads to lowering of the Higgs mass through the very same term. We call this effect λ-doublet mixing. We find that in κSUSY, this is the main effect that lowers the Higgs mass at large λ and small $\tan\beta$, rather than mixing with the singlet, see Fig. 16. This is different from Ref. [52], whose potential contains multiple extra free scales (B_μ, the singlet mass) which are potentially large. (Their benchmark point has $B_\mu \approx 4\mu^2 = (400\text{ GeV})^2$. In this region, λ-doublet mixing accounts for only 15% of the lowering of the Higgs mass below its decoupling limit, Eq. (78); the rest comes from singlet-doublet mixing.) In fact, in κSUSY, $\lambda \sim 2$ is excluded for $\mu \sim 200$ GeV exactly for this reason: the Higgs becomes tachyonic (i.e. the correct electroweak symmetry breaking vacuum disappears).

- The mass of the singlet-like scalar is not really a free parameter. It decouples together with the heavy Higgs ($B_\mu \to \infty$) but not independently. This kind of relation is to be expected in a model with a scale-free superpotential, with $\lambda \sim \kappa$. It is simply an accidental feature (due to the coefficient in $\mathcal{M}^2_{33}$) that the singlet-like scalar is heavier than other scalars by a factor of a few, in the limit of no mixing and $\lambda \sim \kappa$.

- Doublet-singlet mixing now depends on a difference between λ and κ. We find that, although the singlet-like Higgs is not very heavy, this greatly reduces mixing of the Higgs doublet component with the singlet and can lead to decoupling of the SM-like Higgs from the singlet for singlet masses as low as 400 GeV for $\tan\beta \sim 1$.

In the limit of small λ-doublet mixing ($2\lambda^2 v_u v_d < B_\mu + \bar{g}^2 v_u v_d/2$) and negligible doublet-singlet mixing, the tree-level mass of the SM-like Higgs boson is given by

$$m_h^2 \approx M_Z^2 \cos^2 2\beta + \lambda^2 v^2 \sin^2 2\beta. \tag{78}$$

In the appendix, we present analytical formulae for m_h that include both large λ-doublet and singlet-doublet mixings up to second order in an expansion in m_h^2/m_H^2 (light Higgs mass over heavy Higgs mass); we also present the exact solution to m_h in the regime where λ-doublet mixing dominates over doublet-singlet mixing as well as in the opposite case.

In Fig. 17(a), we present contours of the lightest Higgs boson mass, m_h, for typical values of parameters, where we have added the one-loop top-stop contribution with $m_{\tilde{t}} = 450$ GeV and $A_t = 0$. In Fig. 17(b), we show contours of the charged Higgs boson mass, which is given by

$$m_{H^+}^2 = \frac{2B_\mu}{\sin 2\beta} - \lambda^2 v^2 + M_W^2. \tag{79}$$

In the non-decoupling region ($B_\mu/v^2 \gtrsim 1$) and for $\lambda > \sqrt{2}/\sin 2\beta$, the charged Higgs boson can become tachyonic. On the other hand, its mass cannot significantly fall below 300 GeV due to constraints from $b \to s\gamma$. This provides an important constraint on our parameter space and forces us to choose relatively low values of $\lambda \lesssim 1$.

Another potential issue is a light pseudoscalar arising from an approximate R symmetry under which S, H_u, H_d have a charge of 2/3. This symmetry is spontaneously broken by v_s, v_u, v_d so that there is a light R-axion. This axion obtains a mass through loops of gauginos, mixing with other axions, such as the QCD axion, and A_λ, A_κ. In Ref. [84], it was determined that the A terms provide the dominant contribution for $10^{-3} \lesssim |A_{\lambda,\kappa}|/v \ll 1$, which we satisfy. The mass of the R-axion due to the A terms is given in terms of an expansion in $A_{\lambda,\kappa}/v$ by

$$m_{A_1}^2 \approx 9\frac{\mu}{\lambda}\left(\frac{\lambda A_\lambda}{2}\frac{\cos^2\theta_A}{\sin 2\beta} + \frac{\kappa A_\kappa}{3}\sin^2\theta_A\right) + O(A_{\lambda,\kappa}^2), \tag{80}$$

where $\tan\theta_A = \mu/(\lambda v \sin 2\beta) + O(A_{\lambda,\kappa}/v)$. We see that the mass is the geometric mean of μ and $A_{\lambda,\kappa}$ times $O(1)$ factors. Since we generically have $|A_\lambda| > 1$ GeV, the mass is in tens of GeVs, so we are safe from the constraint from Υ decays. Since λ, κ are $O(1)$, however, the Higgs can also decay into the R-axion with a large branching fraction, if this decay mode is kinematically allowed. Assuming $m_h = 125$ GeV, we find that this happens for $|A_\lambda| < 10$ GeV (neglecting A_κ). Depending on parameters, we can have $|A_\lambda| \gtrsim 10$ GeV, in which case decays of the lightest Higgs boson are SM-like.

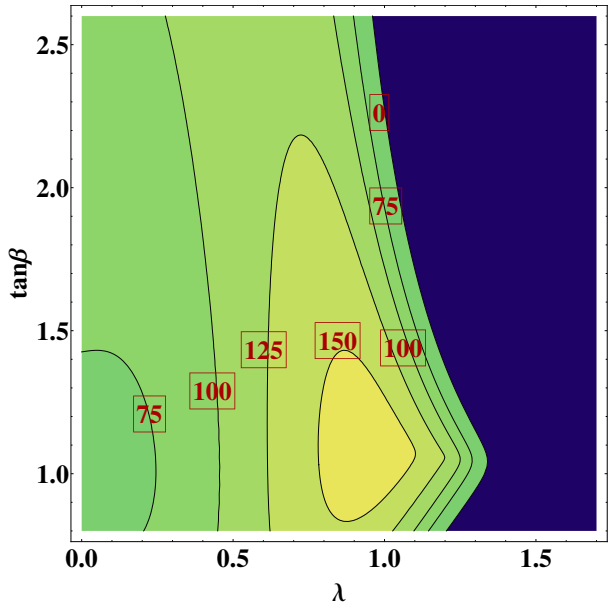

(a) Higgs mass contours, $\kappa = 0.7$, $\mu = 200$ GeV

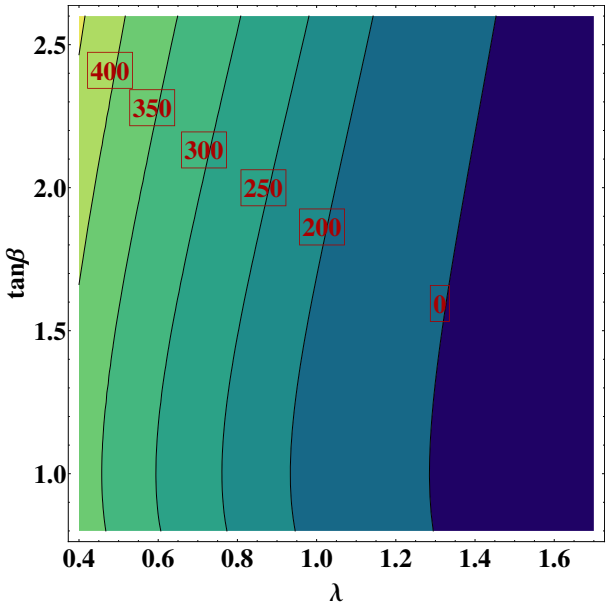

(b) Charged Higgs mass contours, $\kappa = 0.7$, $\mu = 200$ GeV

Figure 17: Left: Contours of the lightest Higgs boson mass in λ-tan β plane. We find the expected rise of the Higgs mass with increasing λ as well as the preference for low tan β. The λ-doublet mixing effect is apparent for large λ where the Higgs mass quickly drops to zero. Right: Contours of the charged Higgs boson mass in the same plane. Relatively low values of λ are forced by the constraint from $b \to s\gamma$, which requires m_{H^+} not much below ~ 300 GeV.

4.3.2 Sample spectra

We here present sample parameter points in κSUSY. To achieve successful electroweak symmetry breaking, in particular to obtain a sufficiently large $\mu = \lambda v_s$, we introduce a negative soft mass-squared for the singlet at k', $m_S^2 \sim -(400 \text{ GeV})^2$. Such a term can arise naturally if there are (additional) messenger fields $f, \bar{f}$ on the IR brane which couple to the S field in the superpotential $W = Sf\bar{f}$ [85]. Here $f, \bar{f}$ are assumed to be SM-gauge singlets and have supersymmetric and supersymmetry breaking masses (roughly) of order k': $M_f \sim \sqrt{F}_f \sim k'$. (This does not require a strong coincidence because the characteristic scale on the IR brane is $k' \sim M'_*$.) The A terms generated by $f, \bar{f}$ loops are small for $M_f \sim \sqrt{F}_f$, since both the A terms and the soft mass-*squared*, m_S^2, are generated at the one-loop order.

We present two sample spectra in Figs. 18 and 19, which correspond respectively to two different choices of the compositeness scale, $k' = 10$ TeV and 1000 TeV. The relevant parameters for electroweak symmetry breaking are λ, κ, m_S^2, and the electroweak gaugino masses $M_{1,2}$. (We choose $m^2_{H_u,H_d,\tilde{Q}_3,\tilde{U}_3}, A_{\lambda,\kappa,t,b} \approx 0$ at k', ignoring loop-suppressed threshold corrections.) The gluino mass is chosen to be small (but still allowed by the experimental constraint) to alleviate

fine-tuning, and the bino is chosen to be the lightest observable-sector supersymmetric particle (LOSP). For the gluino mass we add the one-loop threshold correction, which can be as large as $\approx 20\%$ for the multi-TeV squark masses [86]. In this section, we assume that the gravitino is heavier than the LOSP, so that the bino is the lightest supersymmetric particle. This is the case for $M_{\rm mess} \gtrsim M_{\rm Pl}$, or for $M_{\rm mess} \lesssim M_{\rm Pl}$ if there is additional supersymmetry breaking that does not contribute to the MSSM superparticle masses but pushes up the gravitino mass above the LOSP mass [87]. If the gravitino is lighter than the bino, somewhat stronger bounds on the gluino mass would apply [88]. For example, if the bino decays promptly to the gravitino, then the lower bound is $m_{\tilde{g}} \approx 900$ GeV, instead of ≈ 700 GeV.

In presenting the sample points, we also evaluate the amount of fine-tuning, adopting a conventional criterion [89]

$$\Delta = \max_{i,j} \frac{d \ln A_i}{d \ln B_j}, \tag{81}$$

where $A_i = (m_h^2, v^2)$ and B_j are UV parameters to be specified below. The A_i correspond to the $(\theta_{h,h_u}\hat{v}_u + \theta_{h,h_d}\hat{v}_d + \theta_{h,s}\hat{v}_s)$ and $(\vec{v}_u + \vec{v}_d)/v$ directions in the three-dimensional v_u, v_d, v_s space, respectively, where we define scalar mixing angles in terms of eigenvector overlap: $h = \theta_{h,h_u} h_u + \theta_{h,h_d} h_d + \theta_{h,s} s$. In the case of λ-doublet or singlet-doublet mixing, fine-tuning (e.g. due to stops) may be much alleviated compared to the MSSM due to level repulsion which is generated naturally through large off-diagonal elements in the mass matrix; in the case of singlet-doublet mixing, this has been analyzed in Ref. [52]. We here point out that large-mixing, natural scenarios with TeV-scale stops are typically accompanied by drastic deviations of Higgs couplings, so if the Higgs has only moderate deviations from SM cross sections and decay rates, then naturalness generically requires light stops. In our analysis, we choose $B_j = (\lambda, \kappa, m_S^2, M_{1,2,3}, k', y_t, \tilde{m})$.

3.4.2.1 $k' = 10$ TeV

The following considerations give a bottom-up picture of what is needed to generate a natural superpartner spectrum (in the decoupling regime) [90, 58] that radiatively breaks electroweak symmetry with $k' = 10$ TeV:

- The fine-tuning constraint ($\Delta^{-1} \gtrsim 20\%$) requires $|\mu| \lesssim 210$ GeV, $m_{\tilde{t}} \lesssim 410$ GeV (for degenerate stop masses without mixing), $m_{\tilde{g}} \lesssim 790$ GeV (at the leading-log level; the actual bound is significantly weaker because of the effect of strong interactions), $m_{\tilde{W}} \lesssim 890$ GeV, $m_{\tilde{B}} \lesssim 2800$ GeV, and $\tilde{m} \lesssim 4$ TeV.

- Electroweak symmetry breaking requires $\lambda, \kappa \sim 0.7$ at low energies, as discussed in the last section; we also need $m_S^2 \sim -(400\ \text{GeV})^2$ to generate a sufficiently large μ term.

In Fig. 18, we show a typical mass spectrum for $k' = 10$ TeV, where the lightest Higgs boson mass is evaluated with the one-loop top-stop contribution added. The production cross section

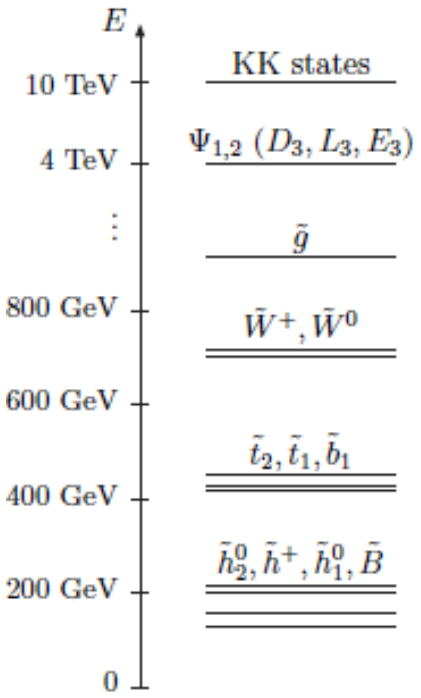

Parameters	Spectrum (GeV)	Properties
$\lambda = 0.66$	$m_h = 125$	$\mu = -201$ GeV
$\kappa = 0.69$	$m_H = 322$	$\tan\beta = 1.97$
$m_S^2 = -(328\text{ GeV})^2$	$m_s = 436$	$\theta_{h,s} = 0.03$
$k' = 10$ TeV	$m_{A_s} = 71$	$\theta_{H,s} = 0.38$
$\tilde{m} = 4$ TeV	$m_A = 367$	$A_\lambda = -21$ GeV
	$m_{H^+} = 329$	$A_\kappa = -2$ GeV
	$m_{\tilde{g}} = 946$	$A_t = 217$ GeV
	$m_{\tilde{W}^+,\tilde{W}^0} = 708$	
	$m_{\tilde{B}} = 127$	
	$m_{\tilde{t}_1} = 431$	
	$m_{\tilde{t}_2} = 467$	
	$m_{\tilde{b}_1} = 416$	
	$m_{\tilde{h}_2^0} = 214$	
	$m_{\tilde{h}^+} = 206$	
	$m_{\tilde{h}_1^0} = 162$	
	$m_{\tilde{s}} = 467$	

Figure 18: A typical mass spectrum for a compositeness scale of $k' = 10$ TeV. The states with mixing are labeled by their largest components. In the left diagram, the states are always ordered from heavy to light. The gluino mass of $m_{\tilde{g}} = 946$ GeV in the table corresponds to $M_3 = 801$ GeV at the scale $m_{\tilde{t}}$ obtained using the MSSM renormalization group evolution. The wino is relatively heavy, which is necessary to generate a mass for the light pseudoscalar $m_{A_s} > m_h/2$ through the A_λ term, in line with recent hints of a Higgs discovery. If the wino is much lighter, the Higgs would decay almost entirely to pseudoscalars.

$\sigma(gg \to h)$ is modified relative to the SM due to non-decoupling stop contributions and A terms; this sample point has an enhancement of 13%. Unlike in the MSSM, the decay rate of the Higgs into $\bar{b}b$ is depleted in λSUSY relative to the SM rate. As expanded in m_h^2/m_H^2, the rate is given by (see the appendix)

$$\frac{\Gamma(h \to \bar{b}b)}{\Gamma_{\rm SM}(h \to \bar{b}b)} = 1 - \tan\beta \, \sin^2 2\beta \, \frac{\lambda v \sqrt{|\lambda^2 v^2 - M_Z^2|}}{2B_\mu}. \tag{82}$$

For the $k' = 10$ TeV spectrum, this formula gives 0.88, within 10% of the exact result, 0.96. Because of this suppression, the branching ratios into other modes are enhanced. In particular, we find that $\mathrm{Br}(h \to \gamma\gamma)$ is increased by 4% with respect to the SM, resulting in an enhancement of $\sigma(gg \to h) \times \mathrm{Br}(h \to \gamma\gamma)$ of 18%. This effect of an enhanced $\gamma\gamma$ signal has been observed for a different parameter space of λSUSY in Ref. [52]; however, here the effect is not large and the decays are practically SM-like. Notice in particular the small mixing of the Higgs with the

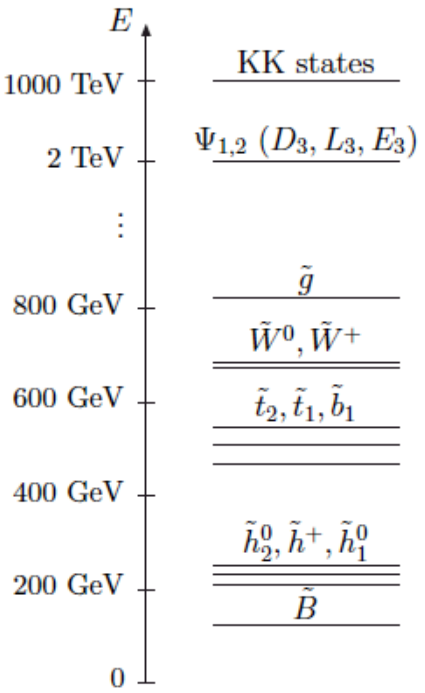

Parameters	Spectrum (GeV)	Properties
$\lambda = 0.66$	$m_h = 125$	$\mu = -242$ GeV
$\kappa = 0.69$	$m_H = 398$	$\tan\beta = 2.12$
$m_S^2 = -(473\text{ GeV})^2$	$m_s = 520$	$\theta_{h,s} = 0.04$
$k' = 1000$ TeV	$m_{A_s} = 95$	$\theta_{H,s} = 0.37$
$\tilde{m} = 2$ TeV	$m_A = 440$	$A_\lambda = -27$ GeV
	$m_{H^+} = 411$	$A_\kappa = -7$ GeV
	$m_{\tilde{g}} = 814$	$A_t = 344$ GeV
	$m_{\tilde{W}^+,\tilde{W}^0} = 677$	
	$m_{\tilde{B}} = 130$	
	$m_{\tilde{t}_1} = 454$	
	$m_{\tilde{t}_2} = 548$	
	$m_{\tilde{b}_1} = 507$	
	$m_{\tilde{h}^0_2} = 255$	
	$m_{\tilde{h}^+} = 247$	
	$m_{\tilde{h}^0_1} = 205$	
	$m_{\tilde{s}} = 546$	

Figure 19: A typical mass spectrum for a compositeness scale of $k' = 1000$ TeV. Definitions are as in Fig. 18. The gluino mass of $m_{\tilde{g}} = 814$ GeV corresponds to $M_3 = 710$ GeV at the scale $m_{\tilde{t}}$ obtained using the MSSM renormalization group evolution.

singlet as anticipated in section 4.3.1. For our $k' = 10$ TeV point, decay rate times branching ratio of both the heavy Higgs and the singlet into WW or ZZ is four orders of magnitude below that of the SM Higgs of the same mass, which makes them invisible to SM Higgs searches. For the fine-tuning parameter, we obtain $\Delta^{-1} = 19\%$, consistent with expectations based on the general argument.

The heavy Higgs decays into A_sA_s, A_sZ, and $\bar{t}t$, with A_s decaying predominantly into $\bar{b}b$. The singlet decays into A_sA_s, A_sZ, $\bar{t}t$, and $\tilde{h}^+\tilde{h}^-$. Due to associated Z production, discovery of these particles may be possible at e^+e^- colliders such as the ILC/CLIC.

3.4.2.2 $k' = 1000$ TeV

The fine-tuning constraint will be more severe for $k' = 1000$ TeV than for $k' = 10$ TeV because of the large $\ln(k'/\text{TeV}) = 6.9$. Performing the same bottom-up analysis as in the case of $k' = 10$ TeV, we find:

- The fine-tuning constraint ($\Delta^{-1} \gtrsim 10\%$) requires $|\mu| \lesssim 290$ GeV, $m_{\tilde{t}} \lesssim 370$ GeV (for degenerate stop masses without mixing), $m_{\tilde{g}} \lesssim 460$ GeV (again at the leading-log level), $m_{\tilde{W}} \lesssim 800$ GeV, $m_{\tilde{B}} \lesssim 2500$ GeV, and $\tilde{m} \lesssim 3.6$ TeV.

For $k' = 1000$ TeV, the theory is expected to be fine-tuned at the 10% level.

In Fig. 19, we show a typical mass spectrum for $k' = 1000$ TeV. We find that, as in the $k' = 10$ TeV case, the phenomenology of the Higgs is mostly SM-like: the production cross section $\sigma(gg \to h)$ is enhanced by 9% relative to the SM; Eq. (82) gives 0.92 as the decay rate of the Higgs to $\bar{b}b$ with respective to the SM, whereas the exact result is 0.96. This translates into an increase of $\sigma(gg \to h) \times \mathrm{Br}(h \to \gamma\gamma)$ of 13% with respect to the SM. As for the heavy Higgs or the singlet, we again find four orders of magnitude suppression of production cross section times branching ratio into WW or ZZ compared to the SM Higgs with the same mass. We find fine-tuning of $\Delta^{-1} = 10\%$ for this sample point, which is in agreement with expectations.

We find that if we relax our requirement of tuning slightly, we can choose k' to be much larger than 1000 TeV without conflicting with Landau pole constraints. We, however, note that two-loop stop contributions to the Higgs quartic are negative and the theory will therefore require larger λ, κ, so it is not obvious that this statement will hold at two loops. Using the tree-level potential as the other extreme to the one-loop potential, one finds that large $\lambda, \kappa \sim 0.8 - 0.9$ are needed to push the Higgs mass high enough and one cannot take k' much higher than 1000 TeV due to Landau pole constraints. The truth is expected to lie somewhere between the tree-level and one-loop situations.

4.4 Flat Space Realization

We now discuss realizing our basic setup, Fig. 1, using a flat space extra dimension. An obvious way to do this is to simply turn off the curvature in models of Section 4.1. The analysis then goes similarly with the replacement $k' \to 1/\pi R$, except that we now do not have a large desert above the compactification scale, $1/R$, so we cannot have the high-scale see-saw mechanism or conventional gauge coupling unification.

In this section, we pursue an alternative realization, adopting supersymmetry breaking by boundary conditions associated with a compact extra dimension [91]. Our model is essentially that in Ref. [92]. Specifically, we consider an $SU(3)_C \otimes SU(2)_L \otimes U(1)_Y$ gauge theory in 5D, with the extra dimension compactified on S^1/Z_2: $0 \le y \le \pi R$. We introduce three generations of matter and Higgs fields in the bulk, but localize the third-generation quark doublet, right-handed top, and Higgs multiplets to the $y = \pi R$ brane:

$$M_{Q_3, U_3, H_u, H_d} \ll -\frac{1}{\pi R}, \tag{83}$$

where M_Φ represents bulk masses as in previous sections. When supersymmetry is broken by twisted boundary conditions with twist parameter α, we obtain

$$m_{\tilde{Q}_3, \tilde{U}_3, H_u, H_d} \ll m_{\tilde{\Psi}_{1,2}, \tilde{D}_3, \tilde{L}_3, \tilde{E}_3} = \frac{\alpha}{R}, \tag{84}$$

at the scale $1/R$, where we have taken

$$|M_{\Psi_{1,2},D_3,L_3,E_3}| \ll \frac{1}{\pi R}. \tag{85}$$

This condition guarantees that the first two generation sfermions are nearly degenerate in mass, avoiding stringent constraints from flavor violation.

To obtain the spectrum we want, we take α/R to be in the multi-TeV region. For the gauge multiplets, we introduce sizable gauge kinetic terms on (one or both of) branes, which control the size of the gaugino masses:

$$M_A = \frac{\pi R g_{4,A}^2}{g_{5,A}^2} \frac{\alpha}{R}, \tag{86}$$

where $g_{5,A}$ and $g_{4,A}$ are the 5D bulk and 4D gauge couplings, respectively, with $g_{4,A}$ given by

$$\frac{1}{g_{4,A}^2} = \frac{\pi R}{g_{5,A}^2} + \frac{1}{\tilde{g}_{0,A}^2} + \frac{1}{\tilde{g}_{\pi,A}^2}, \tag{87}$$

in terms of $g_{5,A}$ and the brane-localized gauge couplings at $y = 0$ and πR, $\tilde{g}_{0,A}$ and $\tilde{g}_{\pi,A}$. We take M_A to be in the sub-TeV region.

Introducing a singlet field S together with the superpotential $\lambda S H_u H_d + f(S)$ on the $y = \pi R$ brane, the analysis of electroweak symmetry breaking goes as in the previous section, with the identification

$$k' \to \frac{1}{\pi R}, \qquad \tilde{m} \to \frac{\alpha}{R}. \tag{88}$$

A negative soft mass-squared for S can be induced, for example, by introducing some bulk field that has a Yukawa coupling to S on the $y = \pi R$ brane.

In the present model, the two circles in Fig. 1 are interpreted as the 5D bulk (left) and the $y = \pi R$ brane (right), rather than the $y = 0$ and πR branes as in previous models. Because of Eq. (85), only a part of the Yukawa hierarchy can be explained by wavefunction profiles. With Eqs. (83, 85) the Yukawa matrices obtain the following structure from the wavefunctions:

$$y_u \sim \begin{pmatrix} \epsilon^2 & \epsilon^2 & \epsilon \\ \epsilon^2 & \epsilon^2 & \epsilon \\ \epsilon & \epsilon & 1 \end{pmatrix}, \qquad y_d \sim \begin{pmatrix} \epsilon^2 & \epsilon^2 & \epsilon^2 \\ \epsilon^2 & \epsilon^2 & \epsilon^2 \\ \epsilon & \epsilon & \epsilon \end{pmatrix}, \qquad y_e \sim \begin{pmatrix} \epsilon^2 & \epsilon^2 & \epsilon^2 \\ \epsilon^2 & \epsilon^2 & \epsilon^2 \\ \epsilon^2 & \epsilon^2 & \epsilon^2 \end{pmatrix}, \tag{89}$$

where $O(1)$ factors are omitted in each element, and $\epsilon \equiv 1/\sqrt{\pi R}$ is the volume dilution factor. The structure beyond this must come from that of 5D Yukawa couplings between matter and Higgs on the $y = \pi R$ brane.

4.5 Conclusions

In this paper we have presented supersymmetric models in which light stops are obtained while keeping near flavor degeneracy for the first two generation sfermions. Such a spectrum is motivated by the naturalness argument together with the recent LHC data. Our construction is

based on the basic picture in Fig. 1: being "close to" electroweak symmetry breaking implies being "away from" supersymmetry breaking, and vice versa. In models where the two sectors correspond to the two branes at the opposite ends of a (warped or flat) extra dimension, the desired superpartner spectra are obtained while reproducing the hierarchy in the Yukawa matrices through wavefunction profiles of the quark/lepton fields. A relatively large Higgs boson mass, including $m_h = 125$ GeV, can be easily accommodated if the scale of Kaluza-Klein excitations is low. For models in warped space, the AdS/CFT correspondence allows us to interpret them in terms of purely 4D theories in which the top and Higgs (and the left-handed bottom) multiplets are composites of some strongly interacting sector. An alternative realization of the picture in Fig. 1 is obtained by identifying the two sectors as the bulk of a flat extra dimension and a brane on its boundary, and by breaking supersymmetry by boundary conditions, which we have also discussed.

In the coming years, the LHC will be exploring the parameter regions of supersymmetric theories in which the stops (and the left-handed sbottom) are light. If electroweak symmetry breaking is indeed natural in the conventional sense, the LHC will find the stops in the sub-TeV region. If not, and if the SM-like Higgs boson is confirmed with $m_h \simeq 125$ GeV, then we would be led to consider that supersymmetry is absent at low energies, or it is realized in a somewhat fine-tuned form, perhaps along the lines of scenarios considered in Refs. [93, 94, 95].

References

[1] ATLAS Collaboration, ATLAS-CONF-2012-019.

[2] CMS Collaboration, CMS-PAS-HIG-12-008.

[3] A. Djouadi, Phys. Rept. **459**, 1 (2008) [hep-ph/0503173].

[4] P. Draper, P. Meade, M. Reece and D. Shih, arXiv:1112.3068 [hep-ph].

[5] L. J. Hall, D. Pinner and J. T. Ruderman, JHEP **1204**, 131 (2012) [arXiv:1112.2703 [hep-ph]].

[6] R. Barbieri, L. J. Hall, Y. Nomura and V. S. Rychkov, Phys. Rev. D **75**, 035007 (2007) [hep-ph/0607332].

[7] R. Harnik, G. D. Kribs, D. T. Larson and H. Murayama, Phys. Rev. D **70**, 015002 (2004) [hep-ph/0311349].

[8] U. Ellwanger, C. Hugonie and A. M. Teixeira, Phys. Rept. **496**, 1 (2010) [arXiv:0910.1785 [hep-ph]].

[9] P. Batra, A. Delgado, D. E. Kaplan and T. M. P. Tait, JHEP **0402**, 043 (2004) [hep-ph/0309149].

[10] A. Maloney, A. Pierce and J. G. Wacker, JHEP **0606**, 034 (2006) [hep-ph/0409127].

[11] P. W. Graham, A. Ismail, S. Rajendran and P. Saraswat, Phys. Rev. D **81**, 055016 (2010) [arXiv:0910.3020 [hep-ph]].

[12] S. P. Martin, Phys. Rev. D **81**, 035004 (2010) [arXiv:0910.2732 [hep-ph]].

[13] U. Ellwanger, JHEP **1203**, 044 (2012) [arXiv:1112.3548 [hep-ph]].

[14] A. Arvanitaki and G. Villadoro, JHEP **1202**, 144 (2012) [arXiv:1112.4835 [hep-ph]].

[15] M. Endo, K. Hamaguchi, S. Iwamoto, K. Nakayama and N. Yokozaki, arXiv:1112.6412 [hep-ph].

[16] ATLAS Collaboration, ATLAS-CONF-2012-007.

[17] T. Appelquist, B. A. Dobrescu and A. R. Hopper, Phys. Rev. D **68**, 035012 (2003) [hep-ph/0212073].

[18] K. Intriligator and M. Sudano, JHEP **1006**, 047 (2010) [arXiv:1001.5443 [hep-ph]].

[19] M. Buican and Z. Komargodski, JHEP **1002**, 005 (2010) [arXiv:0909.4824 [hep-ph]].

[20] E. Salvioni, G. Villadoro and F. Zwirner, JHEP **0911**, 068 (2009) [arXiv:0909.1320 [hep-ph]].

[21] M. S. Carena, J. R. Espinosa, M. Quiros and C. E. M. Wagner, Phys. Lett. B **355**, 209 (1995) [hep-ph/9504316].

[22] G. Cacciapaglia, C. Csaki, G. Marandella and A. Strumia, Phys. Rev. D **74**, 033011 (2006) [hep-ph/0604111].

[23] E. Accomando, A. Belyaev, L. Fedeli, S. F. King and C. Shepherd-Themistocleous, Phys. Rev. D **83**, 075012 (2011) [arXiv:1010.6058 [hep-ph]].

[24] S. Weinberg, Phys. Rev. Lett. **59**, 2607 (1987).

[25] A. H. Guth and E. J. Weinberg, Nucl. Phys. B **212**, 321 (1983); A. Vilenkin, Phys. Rev. D **27**, 2848 (1983); A. D. Linde, Phys. Lett. B **175**, 395 (1986); Mod. Phys. Lett. A **1**, 81 (1986).

[26] R. Bousso and J. Polchinski, JHEP **06**, 006 (2000) [arXiv:hep-th/0004134]; S. Kachru, R. Kallosh, A. Linde and S. P. Trivedi, Phys. Rev. D **68**, 046005 (2003) [arXiv:hep-th/0301240]; L. Susskind, arXiv:hep-th/0302219; M. R. Douglas, JHEP **05**, 046 (2003) [arXiv:hep-th/0303194].

[27] For reviews, see e.g. A. H. Guth, Phys. Rept. **333**, 555 (2000) [arXiv:astro-ph/0002156]; A. Vilenkin, J. Phys. A **40**, 6777 (2007) [arXiv:hep-th/0609193]; S. Winitzki, Lect. Notes Phys. **738**, 157 (2008) [arXiv:gr-qc/0612164]; A. Linde, Lect. Notes Phys. **738**, 1 (2008) [arXiv:0705.0164 [hep-th]].

[28] Y. Nomura, arXiv:1104.2324 [hep-th].

[29] H. Martel, P. R. Shapiro and S. Weinberg, Astrophys. J. **492**, 29 (1998) [arXiv:astro-ph/9701099]; G. Efstathiou, Mon. Not. Roy. Astron. Soc. **274**, L73 (1995).

[30] J. Garriga, M. Livio and A. Vilenkin, Phys. Rev. D **61**, 023503 (2000) [arXiv:astro-ph/9906210]; L. Pogosian and A. Vilenkin, JCAP **01**, 025 (2007) [arXiv:astro-ph/0611573].

[31] R. Bousso, R. Harnik, G. D. Kribs and G. Perez, Phys. Rev. D **76**, 043513 (2007) [arXiv:hep-th/0702115]; J. M. Cline, A. R. Frey and G. Holder, Phys. Rev. D **77**, 063520 (2008) [arXiv:0709.4443 [hep-th]].

[32] A. De Simone, A. H. Guth, M. P. Salem and A. Vilenkin, Phys. Rev. D **78**, 063520 (2008) [arXiv:0805.2173 [hep-th]].

[33] R. Bousso, L. J. Hall and Y. Nomura, Phys. Rev. D **80**, 063510 (2009) [arXiv:0902.2263 [hep-th]].

[34] M. P. Salem, Phys. Rev. D **80**, 023502 (2009) [arXiv:0902.4485 [hep-th]]; R. Bousso and S. Leichenauer, Phys. Rev. D **81**, 063524 (2010) [arXiv:0907.4917 [hep-th]]; R. Bousso, B. Freivogel, S. Leichenauer and V. Rosenhaus, arXiv:1012.2869 [hep-th].

[35] R. Bousso and L. Susskind, arXiv:1105.3796 [hep-th].

[36] E. Komatsu *et al.* [WMAP Collaboration], Astrophys. J. Suppl. **192**, 18 (2011) [arXiv:1001.4538 [astro-ph.CO]].

[37] R. Bousso, B. Freivogel and I. S. Yang, Phys. Rev. D **79**, 063513 (2009) [arXiv:0808.3770 [hep-th]].

[38] W. H. Press and P. Schechter, Astrophys. J. **187**, 425 (1974).

[39] C. Lacey and S. Cole, Mon. Not. Roy. Astron. Soc. **262**, 627 (1993).

[40] G. Kauffmann *et al.* [SDSS Collaboration], Mon. Not. Roy. Astron. Soc. **341**, 54 (2003) [arXiv:astro-ph/0205070].

[41] M. Tegmark, A. Aguirre, M. J. Rees and F. Wilczek, Phys. Rev. D **73**, 023505 (2006) [arXiv:astro-ph/0511774].

[42] A. Cattaneo, A. Dekel, J. Devriendt, B. Guiderdoni and J. Blaizot, Mon. Not. Roy. Astron. Soc. **370**, 1651 (2006) [arXiv:astro-ph/0601295].

[43] C. H. Lineweaver, Icarus **151**, 307 (2001) [arXiv:astro-ph/0012399].

[44] D. A. Fischer and J. Valenti, Astrophys. J. **622**, 1102 (2005); D. Grether and C. H. Lineweaver, Astrophys. J. **669**, 1220 (2007).

[45] R. Maiolino *et al.*, Astron. Astrophys. **488**, 463 (2008) [arXiv:0806.2410 [astro-ph]]; P. S. Behroozi, C. Conroy and R. H. Wechsler, Astrophys. J. **717**, 379 (2010) [arXiv:1001.0015 [astro-ph.CO]].

[46] M. Tegmark and M. J. Rees, Astrophys. J. **499**, 526 (1998) [arXiv:astro-ph/9709058].

[47] J. A. Peacock, Mon. Not. Roy. Astron. Soc. **379**, 1067 (2007) [arXiv:0705.0898 [astro-ph]].

[48] R. Bousso and S. Leichenauer, Phys. Rev. D **79**, 063506 (2009) [arXiv:0810.3044 [astro-ph]].

[49] O. Lahav, P. B. Lilje, J. R. Primack and M. J. Rees, Mon. Not. Roy. Astron. Soc. **251**, 128 (1991).

[50] G. Aad *et al.* [ATLAS Collaboration], arXiv:1109.6572 [hep-ex].

[51] ATLAS report, ATLAS-CONF-2011-163; CMS report, CMS-PAS-HIG-11-032.

[52] L. J. Hall, D. Pinner and J. T. Ruderman, arXiv:1112.2703 [hep-ph].

[53] M. Dine, A. Kagan and S. Samuel, Phys. Lett. B **243**, 250 (1990).

[54] S. Dimopoulos and G. F. Giudice, Phys. Lett. B **357**, 573 (1995) [hep-ph/9507282]; A. Pomarol and D. Tommasini, Nucl. Phys. B **466**, 3 (1996) [hep-ph/9507462]; A. G. Cohen, D. B. Kaplan and A. E. Nelson, Phys. Lett. B **388**, 588 (1996) [hep-ph/9607394].

[55] P. Binétruy and E. Dudas, Phys. Lett. B **389**, 503 (1996) [arXiv:hep-th/9607172]; G. Dvali and A. Pomarol, Phys. Rev. Lett. **77**, 3728 (1996) [arXiv:hep-ph/9607383]; J. Hisano, K. Kurosawa and Y. Nomura, Phys. Lett. B **445**, 316 (1999) [hep-ph/9810411]; Nucl. Phys. B **584**, 3 (2000) [hep-ph/0002286].

[56] For recent work, see e.g. N. Craig, D. Green and A. Katz, JHEP **07**, 045 (2011) [arXiv:1103.3708 [hep-ph]]. R. Barbieri, G. Isidori, J. Jones-Pérez, P. Lodone and D. M. Straub, Eur. Phys. J. C **71**, 1725 (2011) [arXiv:1105.2296 [hep-ph]]; R. Essig, E. Izaguirre, J. Kaplan and J. G. Wacker, JHEP **01**, 074 (2012) [arXiv:1110.6443 [hep-ph]]; R. Auzzi, A. Giveon and S. B. Gudnason, arXiv:1112.6261 [hep-ph].

[57] C. Brust, A. Katz, S. Lawrence and R. Sundrum, arXiv:1110.6670 [hep-ph].

[58] M. Papucci, J. T. Ruderman and A. Weiler, arXiv:1110.6926 [hep-ph].

[59] R. Contino, Y. Nomura and A. Pomarol, Nucl. Phys. B **671**, 148 (2003) [hep-ph/0306259]; G. Burdman and Y. Nomura, Phys. Rev. D **69**, 115013 (2004) [hep-ph/0312247]; Y. Nomura, hep-ph/0410348.

[60] J. Erlich, E. Katz, D. T. Son and M. A. Stephanov, Phys. Rev. Lett. **95**, 261602 (2005) [hep-ph/0501128]; L. Da Rold and A. Pomarol, Nucl. Phys. B **721**, 79 (2005) [hep-ph/0501218].

[61] A. Birkedal, Z. Chacko and Y. Nomura, Phys. Rev. D **71**, 015006 (2005) [hep-ph/0408329].

[62] T. Gherghetta and A. Pomarol, Phys. Rev. D **67**, 085018 (2003) [hep-ph/0302001].

[63] R. Sundrum, JHEP **01**, 062 (2011) [arXiv:0909.5430 [hep-th]].

[64] T. Gherghetta, B. von Harling and N. Setzer, JHEP **07**, 011 (2011) [arXiv:1104.3171 [hep-ph]].

[65] C. Csáki, L. Randall and J. Terning, arXiv:1201.1293 [hep-ph].

[66] N. Craig, M. McCullough and J. Thaler, arXiv:1201.2179 [hep-ph].

[67] S. Krippendorf, H. P. Nilles, M. Ratz and M. W. Winkler, arXiv:1201.4857 [hep-ph].

[68] L. Randall and R. Sundrum, Phys. Rev. Lett. **83**, 3370 (1999) [hep-ph/9905221].

[69] D. Marti and A. Pomarol, Phys. Rev. D **64**, 105025 (2001) [hep-th/0106256]; N. Arkani-Hamed, T. Gregoire and J. Wacker, JHEP **03**, 055 (2002) [hep-th/0101233].

[70] T. Gherghetta and A. Pomarol, Nucl. Phys. B **586**, 141 (2000) [arXiv:hep-ph/0003129].

[71] Y. Nomura, JHEP **11**, 050 (2003) [hep-ph/0309189].

[72] Y. Grossman and M. Neubert, Phys. Lett. B **474**, 361 (2000) [hep-ph/9912408].

[73] G. F. Giudice, M. Nardecchia and A. Romanino, Nucl. Phys. B **813**, 156 (2009) [arXiv:0812.3610 [hep-ph]].

[74] See, e.g., F. Gabbiani, E. Gabrielli, A. Masiero and L. Silvestrini, Nucl. Phys. B **477**, 321 (1996) [hep-ph/9604387]; K. Blum, Y. Grossman, Y. Nir and G. Perez, Phys. Rev. Lett. **102**, 211802 (2009) [arXiv:0903.2118 [hep-ph]].

[75] S. Hamidi and C. Vafa, Nucl. Phys. B **279**, 465 (1987); L. E. Ibáñez, Phys. Lett. B **181**, 269 (1986); N. Arkani-Hamed and M. Schmaltz, Phys. Rev. D **61**, 033005 (2000) [arXiv:hep-ph/9903417].

[76] N. Arkani-Hamed, M. Porrati and L. Randall, JHEP **08**, 017 (2001) [hep-th/0012148]; R. Rattazzi and A. Zaffaroni, JHEP **04**, 021 (2001) [hep-th/0012248].

[77] R. Barbieri, L. J. Hall, Y. Nomura and V. S. Rychkov, Phys. Rev. D **75**, 035007 (2007) [hep-ph/0607332].

[78] G. Aad *et al.* [ATLAS Collaboration], arXiv:1112.3832 [hep-ex].

[79] See, e.g., H. Davoudiasl, S. Gopalakrishna, E. Pontón and J. Santiago, New J. Phys. **12**, 075011 (2010) [arXiv:0908.1968 [hep-ph]]; G. Isidori, Y. Nir and G. Perez, Ann. Rev. Nucl. Part. Sci. **60**, 355 (2010) [arXiv:1002.0900 [hep-ph]], and references therein.

[80] W. D. Goldberger, Y. Nomura and D. R. Smith, Phys. Rev. D **67**, 075021 (2003) [hep-ph/0209158]; T. Gherghetta, Phys. Rev. D **71**, 065001 (2005) [hep-ph/0411090].

[81] A. Brignole, J. A. Casas, J. R. Espinosa and I. Navarro, Nucl. Phys. B **666**, 105 (2003) [hep-ph/0301121]; Y. Nomura, D. Poland and B. Tweedie, Phys. Lett. B **633**, 573 (2006) [hep-ph/0509244].

[82] A. de Gouvêa, A. Friedland and H. Murayama, Phys. Rev. D **57**, 5676 (1998) [hep-ph/9711264].

[83] U. Ellwanger, C. Hugonie and A. M. Teixeira, Phys. Rept. **496**, 1 (2010) [arXiv:0910.1785 [hep-ph]], and references therein.

[84] B. A. Dobrescu and K. T. Matchev, JHEP **09**, 031 (2000) [hep-ph/0008192].

[85] M. Dine, Y. Nir and Y. Shirman, Phys. Rev. D **55**, 1501 (1997) [hep-ph/9607397].

[86] S. P. Martin, Phys. Rev. D **72**, 096008 (2005) [hep-ph/0509115].

[87] Y. Nomura and K. Suzuki, Phys. Rev. D **68**, 075005 (2003) [hep-ph/0110040]; C. Cheung, Y. Nomura and J. Thaler, JHEP **03**, 073 (2010) [arXiv:1002.1967 [hep-ph]].

[88] Y. Kats, P. Meade, M. Reece and D. Shih, arXiv:1110.6444 [hep-ph].

[89] R. Barbieri and G. F. Giudice, Nucl. Phys. B **306**, 63 (1988); J. Ellis, K. Enqvist, D. V. Nanopoulos and F. Zwirner, Mod. Phys. Lett. A **1**, 57 (1986).

[90] R. Kitano and Y. Nomura, Phys. Rev. D **73**, 095004 (2006) [hep-ph/0602096].

[91] A. Pomarol and M. Quirós, Phys. Lett. B **438**, 255 (1998) [hep-ph/9806263]; I. Antoniadis, S. Dimopoulos, A. Pomarol and M. Quirós, Nucl. Phys. B **544**, 503 (1999) [hep-ph/9810410]; R. Barbieri, L. J. Hall and Y. Nomura, Phys. Rev. D **63**, 105007 (2001) [hep-ph/0011311].

[92] R. Barbieri, L. J. Hall and Y. Nomura, Phys. Rev. D **66**, 045025 (2002) [hep-ph/0106190]; Nucl. Phys. B **624**, 63 (2002) [hep-th/0107004].

[93] J. D. Wells, arXiv:hep-ph/0306127; Phys. Rev. D **71**, 015013 (2005) [arXiv:hep-ph/0411041].

[94] N. Arkani-Hamed and S. Dimopoulos, JHEP **06**, 073 (2005) [arXiv:hep-th/0405159].

[95] L. J. Hall and Y. Nomura, JHEP **01**, 082 (2012) [arXiv:1111.4519 [hep-ph]].

A Press-Schechter Formalism and Fitting Functions

The Press-Schechter function F is

$$F(M,t) = \mathrm{erfc}\left(\frac{\delta_c(t)}{\sqrt{2}\,\sigma(M,t)}\right), \tag{90}$$

where $\delta_c(t)$ and $\sigma(M,t)$ are given by [41, 47]

$$\delta_c(t) \simeq \begin{cases} 1.629 + 0.057\, e^{-2.3 G_N \rho_\Lambda t^2} & \text{for } \rho_\Lambda \geq 0 \\ 1.686 + 0.165 \left(\frac{t}{t_{\rm crunch}}\right)^{2.5} + 0.149 \left(\frac{t}{t_{\rm crunch}}\right)^{11} & \text{for } \rho_\Lambda < 0, \end{cases} \tag{91}$$

with $t_{\rm crunch}$ defined in Eq. (22), and

$$\sigma(M,t) \simeq Q\, s(M)\, G(t). \tag{92}$$

Here, Q is the primordial density contrast,

$$s(M) \simeq \left[(9.1\,\mu^{-2/3})^{-0.27} + \left\{50.5\, \log_{10}(834 + \mu^{-1/3}) - 92\right\}^{-0.27}\right]^{-1/0.27}, \tag{93}$$

where $\mu = M\xi^2 G_N^{3/2}$ with $\xi \equiv \rho_{\rm matter}/n_\gamma \simeq 3.7$ eV, and

$$G(t) \simeq \begin{cases} 0.206 \frac{\xi^{4/3}}{\rho_\Lambda^{1/3}} \Big[\tanh^{2/3}(\frac{3}{2} H_\Lambda t)\big\{1 - \tanh^{1.27}(\frac{3}{2} H_\Lambda t)\big\}^{0.82} \\ \qquad + 1.437\big\{1 - \cosh^{-4/3}(\frac{3}{2} H_\Lambda t)\big\}\Big] & \text{for } \rho_\Lambda \geq 0 \\ 0.549\, \xi^{4/3} G_N^{1/3} t^{2/3} \Big[1 + 0.37 \left(\frac{t}{t_{\rm crunch}}\right)^{2.18}\Big]^{-1} \Big[1 - \left(\frac{t}{t_{\rm crunch}}\right)^2\Big]^{-1} & \text{for } \rho_\Lambda < 0, \end{cases} \tag{94}$$

where $H_\Lambda \equiv \sqrt{8\pi G_N|\rho_\Lambda|/3}$.

The function H in the extended Press-Schechter formalism is given by [39, 48]

$$H(t';M,t) = -\int_{M/2}^{M} \frac{M}{M'}\,\frac{d\beta}{dM'}(M',t',M,t)\,dM', \tag{95}$$

where

$$\beta(M_1,t_1,M_2,t_2) = \mathrm{erfc}\left(\frac{1}{Q\sqrt{2(s(M_1)^2-s(M_2)^2)}}\left(\frac{\delta_c(t_1)}{G(t_1)}-\frac{\delta_c(t_2)}{G(t_2)}\right)\right), \tag{96}$$

with $s(M)$ and $G(t)$ defined in Eqs. (93) and (94).

The virial density as a function of time can be fit, following Refs. [41, 48], as the density evolution of a closed universe, according to Birkhoff's theorem. The virial density is then given in terms of the density at turn-around rescaled by the ratio of the volumes, $\rho_{\rm vir} = (R_{\rm vir}/R_{\rm turn})^3\rho_{\rm turn}$. Here, $R_{\rm vir}/R_{\rm turn} \to 2$ at early times ($t \ll 1/H_\Lambda$) as well as for $|\rho_\Lambda| \to 0$ at any fixed t. For positive ρ_Λ, $R_{\rm vir}/R_{\rm turn} = 2/(\sqrt{3}-1) \simeq 2.73$ at late times [49], while for negative ρ_Λ, $R_{\rm vir}/R_{\rm turn} \to 2^{2/3}$ for $t \to t_{\rm crunch}$. Our fit is given by

$$\rho_{\rm vir}(t) \simeq \begin{cases} \left\{\left(18\pi^2\rho_{\rm matter}(t)\frac{\sinh^2(\frac{3}{2}H_\Lambda t)}{(\frac{3}{2}H_\Lambda t)^2}\right)^{1.41} + (40.8\,\rho_\Lambda)^{1.41}\right\}^{\frac{1}{1.41}} & \text{for } \rho_\Lambda \geq 0 \\ \left(18\pi^2\rho_{\rm matter}(t)\frac{\sin^2(\frac{3}{2}H_\Lambda t)}{(\frac{3}{2}H_\Lambda t)^2}\right)\frac{123.6}{123.6+7\left(e^{4.14\frac{t}{t_{\rm crunch}}}-1\right)} & \text{for } \rho_\Lambda < 0, \end{cases} \tag{97}$$

where $\rho_{\rm matter}$ is the matter energy density. This fit is accurate to better than $\approx 5\%$ and 2% for $\rho_\Lambda \geq 0$ and < 0, respectively.[12]

Finally, the time at which most of galaxies of mass M forms, i.e. the solution to Eq. (20), is well approximated by the following fitting function:

$$\tau(M)/{\rm Gyr} \simeq \frac{Q_{\rm obs}^{3/2}}{Q^{3/2}} \begin{cases} 1.880 + c_1(\alpha)\,\tilde{M} + c_3(\alpha)\,\tilde{M}^3 + c_5(\alpha)\,\tilde{M}^5 & \text{for } -10 \lesssim \frac{\rho_\Lambda}{\rho_{\Lambda,{\rm obs}}} < 0 \\ c_0'(\alpha) + c_1'(\alpha)\,\tilde{M} + c_3'(\alpha)\,\tilde{M}^3 + c_5'(\alpha)\,\tilde{M}^5 & \text{for } 0 \leq \frac{\rho_\Lambda}{\rho_{\Lambda,{\rm obs}}} < 10 \\ c_0''(\alpha) + c_1''(\alpha)\,\tilde{M} + c_3''(\alpha)\,\tilde{M}^3 + c_5''(\alpha)\,\tilde{M}^5 & \text{for } 10 \leq \frac{\rho_\Lambda}{\rho_{\Lambda,{\rm obs}}} \lesssim 100, \end{cases} \tag{98}$$

[12]For $\rho_\Lambda < 0$, the approximation leading to Eq. (97), i.e. $\rho_{\rm vir} \gtrsim$ a few $(\rho_{\rm matter}+\rho_\Lambda)$, breaks down for $t/t_{\rm crunch} \gtrsim 0.8$, where we should rather use $\rho_{\rm vir} = 0$ (since there is no stable structure forming). However, since $\rho_{\rm vir}$ in Eq. (97) is small there anyway, using it up to $t/t_{\rm crunch} = 1$ does not lead to a significant error.

where $\alpha = (\rho_\Lambda/\rho_{\Lambda,\rm obs})(Q_{\rm obs}/Q)^3$, $\tilde{M} \equiv \log_{10} \frac{M}{2\times 10^{11} M_\odot}$, and

$$\begin{aligned}
c_1(x) &= -0.311 + 1.276\, e^{0.827\, x} + 1.412 \log_{10}\{1 + |x|^{0.7}\}, \\
c_3(x) &= 0.470 - 0.656\, e^{0.78\, x} - 0.317 \log_{10}(0.2 + |x|), \\
c_5(x) &= -0.0142 + 0.0381\, e^{0.7\, x} + 0.00822 \log_{10}(0.05 + |x|), \\
\\
c_0'(x) &= 1.880 - 0.00205\, x, \\
c_1'(x) &= 0.408 + 0.569\, e^{-1.01\, x} + 0.295 \log_{10}(1 + x), \\
c_3'(x) &= 0.277 - 0.251\, e^{-x} - 0.125 \log_{10}(1 + x), \\
c_5'(x) &= -0.000889 + 0.0151\, e^{-x} - 0.00220 \log_{10}(1 + x), \\
\\
c_0''(x) &= 1.880 - 0.00205\, x, \\
c_1''(x) &= 0.767 - 0.00293\, x - 230\, x^{-4}, \\
c_3''(x) &= -0.530 + 0.000336\, x + 0.847\, x^{-0.1}, \\
c_5''(x) &= 0.106 - 0.0000118\, x - 0.125\, x^{-0.1} - 0.0131\, \log_{10}(-5 + x).
\end{aligned} \tag{99}$$

This fit is accurate to better than $\approx 5\%$ for $M \gtrsim 10^{11} M_\odot$ (but it becomes worse for smaller M, e.g., the accuracy is $\approx 12\%$ at $M \simeq 6 \times 10^{10} M_\odot$). For $100 < \rho_\Lambda/\rho_{\Lambda,\rm obs} < 150$, we use the last expression of Eq. (98), good to the level of $\approx 10\%$; and for $\rho_\Lambda/\rho_{\Lambda,\rm obs} > 150$, we use

$$\rho_{\rm vir}(\tau(M))\,/(10^{-26}\ {\rm g/cm^3}) \simeq (3.66 + 0.032\,\alpha) - (1.36 + 0.0013\,\alpha)\tilde{M}, \tag{100}$$

which is accurate to the level of $\approx 10\%$ up to $\rho_\Lambda/\rho_{\Lambda,\rm obs} \approx 4500$.

B Anthropic Condition from Metallicity

In this appendix, we derive the function n arising from the metallicity constraint, Eq. (23). Suppose that in a merging tree of a galaxy j at time t, j is found to have progenitor galaxies $i = 1, 2, \cdots$ with varying masses M_i at time $t' < t$. Note that this also includes accretion, i.e. matter that was not part of galaxies of appreciable size, since $F(M = 0, t) = 1$ in the Press-Schechter formalism, where accretion is treated as mergers of extremely tiny galaxies with a large galaxy.

Now, let us assume that the relative mass fraction in j that came from i and i' is given by $\frac{dF(M_i,t')}{dM_i} / \frac{dF(M_{i'},t')}{dM_{i'}}$, i.e. the ratio of total amount of baryons at time t' in galaxies of type i and i', respectively. This is true within the Press-Schechter formalism as long as $M_{i,i'} \ll M_j$, since then the overdensities within spherical top-hat regions containing masses $M_{i,i'}$ and M_j are independent of each other at early times. Once $M_{i,i'} \approx M_j$, the assumption is not justified, but in these regimes, there can only be a small amount of merging occurring from i, i' to j, implying little contribution to metallicity. The assumption, therefore, provides a good approximation.

Let x_i $(i = 1, 2, \cdots)$ be the fraction of baryons in the universe that formed stars in halos of mass M_i at time t'. In our simple model, the star formation rate is proportional to the rate of halo

formation for masses $M > M_{\rm min}$ and otherwise zero: $dx_i/dt' \propto \Theta(M_i - M_{\rm min})\, d^2F(M_i,t')/dM_i dt'$. The increase in total metal content summed over galaxies of mass M_i is taken to be proportional to the star formation rate therein, dx_i/dt, so the increase in (linear) metallicity dZ_i is

$$dZ_i(t') \propto \left(\frac{dF(M_i,t')}{dM_i}\right)^{-1} \frac{dx_i}{dt'}\, dt' \propto \left(\frac{dF(M_i,t')}{dM_i}\right)^{-1} \frac{d^2F(M_i,t')}{dM_i dt'}\, \Theta(M_i - M_{\rm min})\, dt', \tag{101}$$

i.e. the total increase in metal content divided by the total mass. The increase in metallicity of galaxy j due to stars at time t', then, has to be weighted by the relative matter fraction of galaxies i, as described above:

$$dZ_j(t') = \frac{\sum_i \frac{dF(M_i,t')}{dM_i}\, dZ_i(t')}{\sum_i \frac{dF(M_i,t')}{dM_i}} \propto \frac{\sum_i \frac{d^2F(M_i,t')}{dM_i dt'}\, \Theta(M_i - M_{\rm min})}{\sum_i \frac{dF(M_i,t')}{dM_i}}\, dt', \tag{102}$$

where we must normalize to the total mass of galaxy j at each time t'.

In the continuum limit, the sum over i becomes an integral over masses. Therefore, the metallicity of galaxy j of mass M at time t is

$$Z(M,t) \propto \int_0^{\tilde{t}} dt'\, \frac{\int_0^M dM'\, \frac{d^2F(M',t')}{dM'dt'}\, \Theta(M' - M_{\rm min})}{\int_0^M dM'\, \frac{dF(M',t')}{dM'}} = \int_0^{\tilde{t}} dt'\, \frac{\frac{d}{dt'}\{F(M_{\rm min},t') - F(M,t')\}}{1 - F(M,t')}, \tag{103}$$

where $\tilde{t} = \min\{t, \tilde{t}_{\rm stop}\}$. The constraint that one cannot accumulate negative metallicity determines the timescale $\tilde{t}_{\rm stop}$ as a solution to

$$\frac{d}{dt'}\{F(M_{\rm min},t') - F(M,t')\}\Big|_{t'=\tilde{t}_{\rm stop}} = 0, \tag{104}$$

at which time merging of galaxies of mass $M_{\rm min} < M' < M$ into those more massive than M begins to dominate over formation of new galaxies in this mass region. Since merging into larger structures is also occurring at earlier times, one expects that we slightly underestimate the metallicity. However, in practice, the formation of new galaxies in this mass range and mergers into structures beyond are well separated in time, so a simple cutoff at $\tilde{t}_{\rm stop}$ is sufficient.

Now, since $F(M,t') \le F(M,\tilde{t}_{\rm stop}) = \mathrm{erfc}(1/\sqrt{2}) \simeq 0.317$, the denominator of Eq. (103) is always between 0.68 and 1; in fact, it is very close to 1 in most of the parameter regions. Therefore, we can safely ignore the denominator of Eq. (103) and obtain

$$Z(M,t) \propto \big(F(M_{\rm min},\tilde{t}) - F(M,\tilde{t})\big). \tag{105}$$

In general, the probability of forming planets is expected to be proportional to some power m of the metallicity [43, 44]. This gives

$$n(M,t) = Z(M, t - t_{\rm evol})^m, \tag{106}$$

which is Eq. (23) in the text.

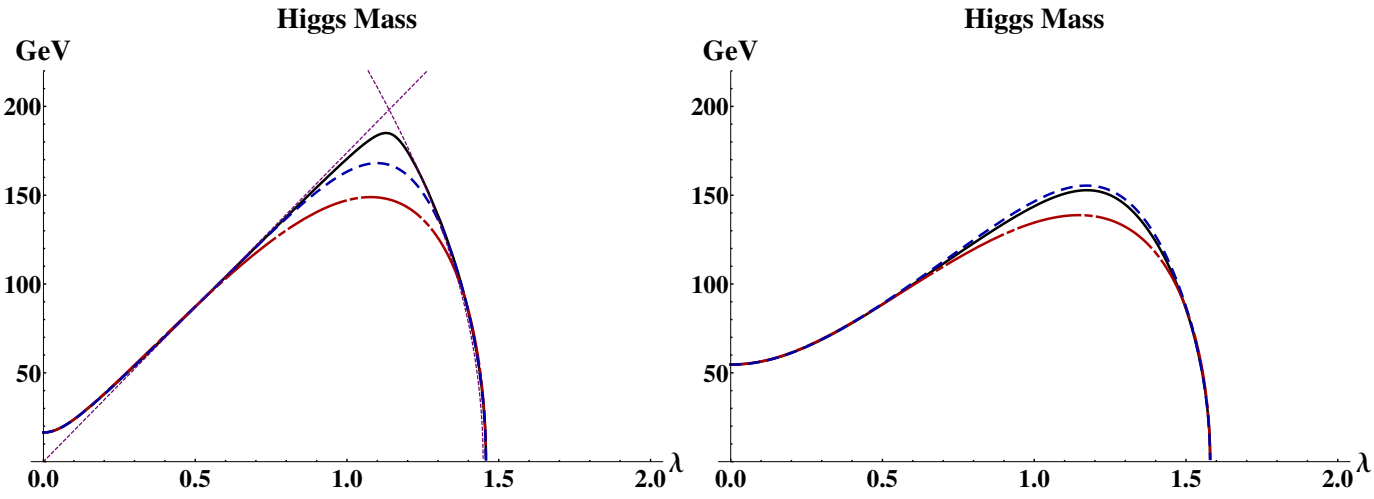

(a) $\tan\beta = 1.2$, $\kappa = 1.0$, $\mu = 200$ GeV (b) $\tan\beta = 2.0$, $\kappa = 1.0$, $\mu = 200$ GeV

Figure 20: The Higgs boson mass as a function of λ for fixed values of $\tan\beta$ and κ, given by the exact tree-level formula (black, solid line), the first-order (red, dot-dashed) and second-order (blue, dashed) analytical formulae in Eqs. (107, 108). On the left, the piece-wise exact analytical solutions for $\tan\beta = 1$ are also shown as magenta, dotted lines. The second-order formula gives a very good fit away from the point $\tan\beta = 1$, $\lambda = \lambda_{\rm crit}$ where the dotted lines cross.

C Analytical Formulae for the Higgs Boson Mass

We first describe the effects of λ-doublet mixing in the non-decoupling regime, $2\lambda^2 v_u v_d \sim B_\mu + v_u v_d \bar{g}^2/2$, in terms of an expansion in m_h^2/m_H^2 (light Higgs mass over heavy Higgs mass) up to second order. For this purpose, we suspend doublet-singlet mixing in this paragraph; it will be discussed below. We find that to first order in the above mentioned expansion, the light Higgs mass is given by

$$m_h^2 \approx M_Z^2 \cos^2 2\beta + \lambda^2 v^2 \sin^2 2\beta \left(1 - \frac{\lambda^2 v^2 - M_Z^2}{2B_\mu} \sin 2\beta\right), \tag{107}$$

where we have used the zeroth order result $m_H^2 = 2B_\mu/\sin 2\beta$. This approximation is valid to within 10% for $\tan\beta \gtrsim 2$ with $\kappa = 1$, $\mu = 200$ GeV. Performing the expansion to second order in m_h^2/m_H^2, we obtain

$$m_h^2 \approx m_{h,0}^2 \, \frac{2B_\mu - M_Z^2 \sin 2\beta}{2B_\mu - m_{h,0}^2 \sin 2\beta}, \tag{108}$$

where $m_{h,0}^2$ is given by Eq. (107). We find that this second-order expansion gives the correct Higgs mass to within 2%, 5%, and 10% for $\tan\beta > 2$, 1.4, and 1.2, respectively, with $\kappa = 1$, $\mu = 200$ GeV. The analytical formulae are compared with the exact tree-level values in Fig. 20. As $\tan\beta$ approaches one, the gap between the light and heavy Higgs masses shrinks to zero at

a value of $\lambda = \lambda_{\rm crit}$ given by $\lambda_{\rm crit}^2 v^2 = B_\mu + M_Z^2/2$. This kink-structure cannot be faithfully described by a perturbative expansion in m_h^2/m_H^2. For $\tan\beta = 1$, Eq. (78) is an exact solution for $\lambda < \lambda_{\rm crit}$, while $m_h^2 = 2B_\mu + M_Z^2 - \lambda^2 v^2$ for $\lambda > \lambda_{\rm crit}$. In the case of a large Higgs mass, $m_h^2 \gg M_Z^2$, a useful expression is

$$m_h^2 = \frac{1}{2}\left(\frac{B_\mu}{\sin\beta\cos\beta} - \sqrt{(2\lambda^2 v^2 \sin 2\beta - 2B_\mu)^2 + 4B_\mu^2 \cot^2 2\beta}\right). \tag{109}$$

We now give an analytic formula for the correction to the Higgs mass from mixing with the singlet in the limit of negligible λ-doublet mixing, $2\lambda^2 v_u v_d \ll B_\mu + \bar{g}^2 v_u v_d/2$, which corresponds to the doublet-doublet decoupling regime. Performing again an expansion in m_h^2/m_s^2, with m_s^2 the $\mathcal{M}_{33}^2$ entry of the scalar mass matrix, one finds to first order

$$\delta m_h^2 = -\frac{4\mu^2 v^2}{m_s^2}\left(\lambda - \left(\kappa + \lambda\frac{A_\lambda}{2\mu}\right)\sin 2\beta\right)^2. \tag{110}$$

In the limit $A_{\lambda,\kappa} \to 0$, this agrees with the result in Ref. [83].